Available online at www.sciencedirect.com
SCIENCE DIRECT®
International Journal of Thermal Sciences 44 (2005) 735–755
International Journal of Thermal Sciences
www.elsevier.com/locate/ijts

Numerical study of the thermal degradation of isotropic and anisotropic polymeric materials ☆

E. Soler [a], J.I. Ramos [b,*]

[a] *Departamento de Lenguajes y Ciencias de la Computación, ETSI Informática, Universidad de Málaga, 29071 Málaga, Spain*
[b] *Room I-320-D, ETS Ingenieros Industriales, Universidad de Málaga, Plaza El Ejido, s/n, 29013 Málaga, Spain*

Received 4 August 2004; received in revised form 10 January 2005; accepted 14 January 2005

Available online 12 April 2005

Abstract

The thermal degradation of two-dimensional isotropic, orthotropic and anisotropic polymeric materials is studied numerically by means of a second-order accurate (in both space and time) linearly implicit finite difference formulation which results in linear algebraic equations at each time step. It is shown that, for both isotropic and orthotropic composites, the monomer mass diffusion tensor plays a role in initiating the polymerization kinetics, the formation of a polymerization kernel and the initial front propagation, whereas the later stages of the polymerization are nearly independent of the monomer mass diffusion tensor. In anisotropic polymeric composites, it has been found that the monomer mass diffusion tensor plays a paramount role in determining the initial stages of the polymerization and the subsequent propagation of the polymerization front, the direction and speed of propagation of which are found to be related to the principal directions of both the monomer mass and the heat diffusion tensors. It is also shown that the polymerization time and temperatures depend strongly on the anisotropy of the mass and heat diffusion tensors.

Keywords: Polymerization; Isotropic composites; Anisotropic composites; Linearly implicit method; Thermal degradation; Curing

1. Introduction

Thermal degradation of polymeric materials is a consequence of the fact that all organic macromolecules as well as low-molecular weight organic molecules are stable only below a certain temperature threshold which is much lower than that of many inorganic materials. Since molecules consist of atoms linked together by covalent bonds, and the strength of these bonds is limited, a high thermal sensitivity of organic substances can be explained at the molecular level because of the scissions of chemical bonds under the influence of heat are the result of overcoming the bond dissociation energies. Methodologies based on tracing the time-and-rate dependent thermochemical and viscometric properties of polymers back to the origin at their molecular level are computationally costly and impractical for routine engineering applications [1]. On the other hand, analytical methods fail in detecting chemical changes in polymers induced by their thermal degradation. Under these circumstances, the development of macroscopic mathematical models which incorporate the nonlinear coupling between chemical kinetics and heat transfer and allow for the prediction of thermal degradation as a function of space and time has become an important and challenging engineering task [2].

In this paper, we propose a model for the curing of thermoset resins which is the key process in the manufacture of polymeric materials. These materials embrace a variety of applications including polymeric composites, elastomers, thermosets, thermoplastics, polymer colloids, coatings, films, polymer blends, and polymeric biomaterials. For

☆ A preliminary version of this paper was presented at CHT-04: An ICHMT International Symposium on Advances in Computational Heat Transfer, April 2004, G. de Vahl Davis and E. Leonardi (Eds.), CD-ROM Proceedings, ISBN 1-5670-174-2, Begell House, New York, 2004.

* Corresponding author. Tel.: +34-95-2131402; fax: +34-95-2132816.
E-mail addresses: esc@lcc.uma.es (E. Soler), jirs@lcc.uma.es (J.I. Ramos).

1290-0729/$ – see front matter
doi:10.1016/j.ijthermalsci.2005.01.009

example, thermosetting materials require more delicate techniques at the processing stage than conventional thermoplastics, but this is paid off by the fact that the resulting materials are more stable in terms of creeping and softening at high temperatures. As a result, thermoset composites are highly demanded in areas such as the encapsulation of computer chips, communication industry, biomedical applications, etc. [3–5].

The curing of thermoset resins is a highly irreversible and complex process which requires accounting for many features such as the molecular weight dependence of the stress relaxation modulus (which plays a paramount role in understanding the effects of viscosity in polymers), the high sensitivity of the viscosity on temperature, the non-Newtonian rheological properties of the molten polymer, the generation of high stresses which may contribute to material failure, etc. In this paper, we focus on the modelling and numerical simulation of the thermochemical properties of thermosets; the model developed here can be improved at a later stage by including a model of the mechanical properties of thermosets and, in particular, the prediction of shrinkage during thermoset curing. Our main assumption is based on the fact that the behavior and properties of polymeric materials are determined largely by heat and mass transfer processes which, in turn, depend strongly on the degradation reactions. Since the polymerization kinetics in thermoset composites during the cure is a fairly complex process due to the fact that the curing kinetics is determined by cross-linking and the dynamics of the heat generation response, we consider here a polymerization kinetics model that takes into account the nonlinear coupling between heat and mass transfer, the anisotropic diffusion of both heat and monomer mass, and the quenching of the reaction if the temperature is not high enough. Current models of thermoset curing include heat diffusion, assume isotropic heat diffusion even in the case of composite materials, may consider the dependence of the thermal capacity or specific heat with temperature, and account for the resin cure or conversion by means of an ordinary differential equation for the resin conversion rate which depends in a polynomial fashion on the resin concentration, but they ignore the resin diffusion and consider isotropic heat diffusion [2,6].

In this paper, resin diffusion is included, the thermal capacity and the monomer mass and heat diffusivity tensors are assumed to be independent of the temperature, and the diffusion coefficients of both heat and monomer mass may be anisotropic. The resin conversion rate during the curing process can be obtained from the spatial integration of the mass balance equation which contains diffusion and a nonlinear reaction term that depends in an Arrhenius fashion on the temperature, while the energy equation contains a nonlinear term that is linearly proportional to the chemical reaction rate and the total heat of reaction of the thermoset, i.e., the heat of polymerization. The pre-exponential factor and the activation energy of the reaction rate are assumed to be independent of both the resin concentration and temperature. As a consequence of these assumptions, the model for the thermal degradation of polymeric materials presented in this paper consists of two two-dimensional, nonlinearly coupled reaction–diffusion equations for the resin mass concentration and the temperature of the thermoset resin which include anisotropic heat and monomer mass diffusion and are analogous to those appearing in the combustion of anisotropic solid media. The inclusion of resin diffusion is novel in thermal degradation processes and accounts for mass transfer induced by concentration gradients, but has been neglected in the past because it was considered to be a slow process and because of the absence of reliable diffusion data in polymeric materials, especially composite ones. It should be pointed out that resin diffusion also takes place due to thermal gradients and that the gradients of the resin mass concentration also affect the heat diffusion in an analogous manner to the Soret and Dufour effects in coupled heat and mass transfer processes [7–9]; the effects of both thermal and mass gradients on mass and heat diffusion, respectively, are not considered in this paper. Furthermore, the advective terms in the resin mass concentration and energy equation are neglected because of the small mass and energy Péclet numbers considered in this study. In addition, the heat and monomer mass diffusion terms were considered to be constant, and the thermal capacity was assumed to be independent of both the temperature and the resin conversion or cure.

Studies of resin transfer molding processes that include advective terms in the energy conservation equation and the degree of curing, e.g., [10,11], assume that the resin is an incompressible fluid, the velocity field of which is governed by Darcy's law, i.e., the velocity field is proportional to the pressure gradient and the proportionality factor depends on the fluid dynamic viscosity and the permeability tensor, and employ either ordinary differential equations for the curing degree [10] or transport equations for the chemical species [11]. These models do require a knowledge of the volume fraction and the permeability tensor which are usually determined from experimental measurements, and, in some cases, are based on nonplausible assumptions such as the assumption of local thermal equilibrium between the solid and liquid phases. These models reduce to the one employed here whenever the thermal and Péclet numbers are small, i.e., whenever advection is much smaller than diffusion.

The paper has been organized as follows. In Section 2, we present the equations governing the heat and mass transfer processes that occur in the curing of resins. The reaction kinetics employed in this section is rather simplified but contains the main ingredients that characterize combustion, self-propagating high temperature synthesis, thermal autocatalysis, solid combustion, free-radical polymerization and epoxy curing processes [12–17]. As a consequence, the formulation presented in the paper can be used to study a variety of processes different from the thermal degradation of polymeric materials considered in this paper. In Section 3, a detailed description of the numerical method employed to

study the thermal degradation of anisotropic polymeric materials is presented, and, in Section 4, a rather detailed study of the thermal degradation of anisotropic polymeric materials is considered. Finally, a brief section summarizes the main conclusions of the paper.

2. Formulation

As stated in the Introduction, the objective of this study is to analyze numerically the two-dimensional thermal degradation of anisotropic polymeric materials by accounting for the diffusion of both heat and monomers. However, since the thermal degradation of polymeric materials is governed by a set of two nonlinearly-coupled reaction–diffusion equations and is, therefore, governed by the same type of equations that characterize combustion, self-propagating high temperature synthesis, thermal autocatalysis, free-radical polymerization and epoxy curing processes [12–17], we present a general formulation which can also be applied to study these processes.

Our main assumption is based on the fact that the behavior and properties of polymeric materials are mainly determined by heat and mass transfer processes which depend on the degradation kinetics. However, since the thermal degradation of polymeric composites during the cure is a complex process due to the fact that the cure is determined by cross-linking and heat generation, we have employed a simplified first-order kinetics model and taken into consideration the diffusion of both heat and monomers. The model can be written in nondimensional form as

$$\frac{\partial u}{\partial t} = \nabla \cdot (\mathbf{D} \cdot \nabla u) - R(u, v) \quad 0 < x < L_x,\ 0 < y < L_y,\ t > 0 \tag{1}$$

$$\frac{\partial v}{\partial t} = \nabla \cdot (\mathbf{K} \cdot \nabla v) + qR(u, v) \quad 0 < x < L_x,\ 0 < y < L_y,\ t > 0 \tag{2}$$

where t is time, $\nabla u = (\frac{\partial u}{\partial x}, \frac{\partial u}{\partial y})$, x and y are Cartesian coordinates, L_x and L_y are the dimensions in the x- and y-directions, respectively, $R(u, v)$ is the reaction rate, q is the heat of polymerization, u and v denote the mass concentration of monomers and the temperature, respectively, $\mathbf{D}$ and $\mathbf{K}$ denote the monomer and heat diffusion tensors, respectively. These tensors are assumed to be symmetric, and positive-definite in order to ensure elliptic behavior under steady-state conditions. The components of these tensors are D_{ij} and K_{ij} and are assumed to be constant, and the reaction rate can be expressed as

$$R(u, v) = \alpha u e^{-\beta/v} \tag{3}$$

where α and β are a Damkhöler number and the nondimensional activation energy, respectively. Note that the formulation presented here assumes that the thermal capacity and the monomer and heat diffusion tensors are independent of both the temperature and monomer concentration. This assumption may not be a realistic one when considering the curing of polymeric materials where the thermal capacity is known to depend on the temperature, e.g., [2,6], but, as stated above, our main objective in this study is to examine the effects of the anisotropy of the monomer and heat diffusion tensors on the thermal degradation of polymeric materials. Moreover, the numerical method presented here can easily handle the dependence of the thermal capacity on temperature, monomer concentration, space and time, and calculations performed with more realistic, i.e., temperature-dependent, specific heats or thermal capacities may be performed in the future. Furthermore, many studies on the curing of polymeric materials and frontal polymerization also assume that the specific heat is constant, e.g., [17–22], although mathematical models of frontal polymerization involve initiation, propagation and termination of the chain polymerization. Initiation involves two steps; in the first one, the initiator decomposes into two active radicals, while, in the second step, the radical species attach to their respective monomers to form live monomer radicals. In the propagation step, the monomer and the live monomer radical react and form live polymer chains. These chains continue to grow until two live polymer chains of the same type attach to each other to terminate the reaction. These kinetics processes are usually modelled by means of six ordinary differential equations for the initiator, primary free radicals, monomer concentrations, and the concentrations of the live monomer radicals of different lengths, by means of Arrhenius-type equations [20]. By way of contrast, the kinetics employed in this study of thermal degradation of polymeric materials and composites only involves a single-step overall chemical reaction which is of first-order in the monomer concentration, i.e., the reaction rate is proportional to the monomer concentration and the proportionality constant is given by an Arrhenius expression.

The reaction kinetics considered in this study is of first-order in the monomer concentration and differs from that employed in other studies which assumed that the conversion of monomers [2], i.e., $G = 1 - u$, is governed by

$$\frac{\mathrm{d}G}{\mathrm{d}t} = KG^{\gamma_1}(G_{\max} - G)^{\gamma_2}(1 - G)^{\gamma_3} \tag{4}$$

where $K = K_0 \exp(-E/RT)$, K_0 is a constant, T is the dimensional temperature, R is the universal gas constant, E is the activation energy and the exponents γ_1, γ_2 and γ_3 are constant which are determined from experimental data.

A comparison between Eqs. (1) and (4) indicates that the latter accounts for the conversion of monomers by means of an ordinary differential equation, but neglects the diffusion of monomers, whereas the former employs a more complex reaction kinetics than the latter. Note, however, that many other researchers have also used a first-order polymerization kinetics albeit disregarding the diffusion of monomers in their studies of polymer curing [17], deprotection reaction of polymers and the diffusion of acids in chemically

amplified resists [24] and frontal polymerization [18]. Costa et al. [19] accounted for the diffusion of monomers in their one-dimensional steady-state studies of styrene polymerization in tubular reactors, assumed that the polymer does not diffuse, considered a polymerization kinetics which is thermally initiated and is terminated by combination, and a thermal conductivity that is a function of the temperature and monomer concentration, whereas Kosar and Gomzi [23] neglected monomer diffusion in their one-dimensional studies of polyester thermosets curing in cylindrical-polar coordinates, used an Arrhenius reaction rate model which is similar to Eq. (4), and assumed constant thermal capacity and heat conductivity.

In this paper, unless stated otherwise, $L_x = 60$, $L_y = 20$, $q = 200$, $\alpha = 3.52 \times 10^{-2}$, $\beta = 40$, and the boundaries were considered to be adiabatic for both the monomer concentration and the temperature, i.e.,

$$(\mathbf{D} \cdot \nabla u) \cdot \mathbf{n} = 0, \qquad (\mathbf{K} \cdot \nabla v) \cdot \mathbf{n} = 0, \quad \text{on } \partial D \tag{5}$$

where $\mathbf{n}$ denotes the unit outward normal to the boundary. As an example, the boundary condition for u at $x = 0$ is $D_{11}\frac{\partial u}{\partial x}(0, y, t) + D_{12}\frac{\partial u}{\partial y}(0, y, t) = 0$.

The nondimensional values of the heat of reaction, pre-exponential factor and activation energy, i.e., q, α and β, respectively, employed in this study are typical in combustion, curing of polymeric materials, self-propagating high temperature synthesis, thermal autocatalysis, solid combustion, free-radical polymerization and epoxy curing processes [12–17]. It must be noted, however, that, in some of these phenomena, the pre-exponential factor may be a function of the temperature.

Initially, $u(0, x, y) = 1$ and $v(0, x, y) = 0$ which corresponds to zero reaction rate, i.e., the cold boundary difficulty [12] has been avoided. However, in order to start the polymerization process, a source term, $S(t, x, y)$ was added to the energy equation in such a manner that $S \equiv 0$ for $x_{\mathrm{BI}} > x$, $x > x_{\mathrm{SI}}$, $y_{\mathrm{BI}} > y$, $y > y_{\mathrm{SI}}$, $S = \varepsilon t$ for $0 \leqslant t \leqslant t_{\mathrm{OFF}}$ and $x_{\mathrm{BI}} \leqslant x \leqslant x_{\mathrm{SI}}$ and $y_{\mathrm{BI}} \leqslant y \leqslant y_{\mathrm{SI}}$, $S = \varepsilon(2t_{\mathrm{OFF}} - t)$ for $t_{\mathrm{OFF}} \leqslant t \leqslant 2t_{\mathrm{OFF}}$ and $x_{\mathrm{BI}} \leqslant x \leqslant x_{\mathrm{SI}}$ and $y_{\mathrm{BI}} \leqslant y \leqslant y_{\mathrm{SI}}$, and $S \equiv 0$ for $t > t_{\mathrm{OFF}}$, where $v(t_{\mathrm{OFF}}, x, y) = 12$, i.e., t_{OFF} is the time at which the temperature within the compact heat source employed in this study exceeds a threshold value equal to 12, and $\varepsilon = 1.2/20$. Here, $(x_{\mathrm{BI}}, y_{\mathrm{BI}}) = (5.1, 10)$, $x_{\mathrm{SI}} = 5.4$ and $y_{\mathrm{SI}} = 10.4$.

The source term for starting the polymerization reactions used in this paper is analogous to the heat sources used in combustion theory to simulate ignition phenomena [12,13] and has compact support in both space and time, i.e., it is different from zero in a small spatial region for a finite time. The heat source employed here can also be used to study stereolithography where polymer curing of the polymer is achieved by exposing small zones to laser irradiation [17]. In addition, as shown below, the temperature spikes that occur in the curing of polymeric composites can be controlled by exposing them to additional heat sources such as, for example, laser irradiation.

3. Numerical method

Eqs. (1) and (2) were discretized by means of a second-order accurate Crank–Nicolson method in time and the non-linear terms were linearized with respect to the previous time level. As a consequence, the following linear elliptic partial differential equation was obtained at each time step

$$\begin{aligned} &\frac{\Delta \mathbf{U}}{\Delta t} - \frac{1}{2}\nabla \cdot (\mathbf{Q} \cdot \nabla \Delta \mathbf{U}) - \frac{1}{2}\mathbf{J}^n \Delta \mathbf{U} \\ &\quad = \nabla \cdot \left(\mathbf{Q} \cdot \nabla \mathbf{U}^n\right) + \mathbf{S}^n\left(\mathbf{U}^n\right) \\ &\quad 0 < x < L_x,\ 0 < y < L_y \end{aligned} \tag{6}$$

where Δt is the time step, $\mathbf{U} = (u, v)^{\mathrm{T}}$, $\Delta \mathbf{U} = \mathbf{U}^{n+1} - \mathbf{U}^n$, $\mathbf{J} = \frac{\partial \mathbf{S}}{\partial \mathbf{U}}$, $\mathbf{U}^n = \mathbf{U}(x, y, t^n)$, $\mathbf{Q} = \left(\begin{smallmatrix} \mathbf{D} & \mathbf{0} \\ \mathbf{0} & \mathbf{K} \end{smallmatrix}\right)$ is related to the diffusion tensors $\mathbf{D}$ and $\mathbf{K}$, the superscript T denotes transpose, and the superscript n denotes the nth time level, i.e., $t^n = n\Delta t$. In the results presented in this paper, $\Delta t = 0.01$, unless stated otherwise.

The linear elliptic Eq. (6) was discretized by means of central differences in an equally-spaced grid in the x- and y-directions at both the interior and the boundary points. The boundary conditions were implemented by using fictitious grid points as follows. At the left boundary, i.e., $x = 0$, for example, the second-order accurate discretization of the boundary condition for u yields

$$u_{0,j} = u_{2,j} - \frac{D_{12}\Delta x}{D_{11}\Delta y}(u_{1,j+1} - u_{1,j-1}) \tag{7}$$

where $x = 0$, $y = 0$ and $y = L_y$ corresponds to $i = 1$, $j = 1$ and $j = NJ$, respectively, NJ denotes the number of grid points in the y-direction, $i = 0$ corresponds to a line of fictitious points, and Δx and Δy are the grid spacings in the x- and y-directions, respectively. Eq. (7) is applicable for $j = 2, 3, \ldots, NJ - 1$. At the corner points, e.g., $(x, y) = (0, 0)$ and $(0, L_y)$, i.e., $(i, j) = (1, 1)$ and $(1, NJ)$, Eq. (5) implies that $\frac{\partial u}{\partial x}$, $\frac{\partial v}{\partial x}$ $\frac{\partial u}{\partial y}$ and $\frac{\partial v}{\partial y}$ are nil and, therefore, equations analogous to Eq. (7) demand that $u_{0,1} = u_{2,1}$, $u_{1,0} = u_{1,2}$ $u_{0,NJ} = u_{2,NJ}$, and $u_{1,NJ+1} = u_{1,NJ-1}$. Similar conditions apply to the other boundaries and corner points.

The discretization of Eq. (6) at the interior points and at the boundaries together with the replacement of the unknown values at the fictitious points in terms of those at the interior and boundaries provides a system of linear algebraic equations which was solved by means of the BiCGStab algorithm [25]. In most of the results presented in this paper, the number of grid points in the x- and y-directions was $NI = 201$ and $NJ = 51$, respectively, so that $\Delta x = 0.3$ and $\Delta y = 0.40$. It must be noted, however, that many numerical studies were performed to assess the effects of the spatial and temporal step sizes on the results taking into consideration the heat supplied by the source to initialize the polymerization process, and that very few differences were observed between the results corresponding to $\Delta t = 0.01$ and 0.001, and grids which employed $\Delta x = 0.3$ and 0.15, and $\Delta y = 0.40$ and 0.20; thus, unless stated otherwise, the results presented in this section correspond to $\Delta x = 0.3$, $\Delta y = 0.40$ and

$\Delta t = 0.01$. Moreover, the implicit, time-linearized method presented in this paper is (linearly) stable and second-order accurate in both space and time, corresponds to a single iteration of the Newton–Raphson procedure, and has been used in numerous studies on two-dimensional reaction–diffusion equations [8,9,26–28].

4. Results

Many numerical simulations have been performed to determine the effects of the monomer mass and heat diffusion tensors on the thermal degradation/curing of polymeric composites. These simulations can be classified in two main groups: those that account for the diffusion of monomers and those for which $\mathbf{D} = \mathbf{0}$. The first can be further classified into five subgroups: isotropic heat and monomer mass diffusion, orthotropic heat diffusion and isotropic monomer mass diffusion, isotropic heat diffusion and orthotropic monomer mass diffusion, orthotropic heat and monomer mass diffusion, and anisotropic diffusion where at least one of the diffusion tensors is anisotropic, i.e., either K_{ij} or D_{ij} is different from zero for $i \neq j$. Orthotropic tensors are those for which $K_{ij} = 0$ if $i \neq j$ and $K_{11} \neq K_{22}$. Due to the large number of simulations performed (cf. Tables 1 and 2), we can only show here some sample results. In addition, calculations were performed to determine the effects of the heat of reaction, pre-exponential factor and activation energy on the thermal degradation of polymeric materials, as discussed in the following subsections.

4.1. Thermal degradation with monomer diffusion

Fig. 1 illustrates the temperature at selected times for the isotropic cases 1, 2 and 3, and indicates that the polymerization front propagates faster in case 2 than in cases 1 and 3; however, the differences between cases 1 and 2 are small, thus indicating that the monomer diffusion is not very important for these two cases. The results corresponding to case 3 show that, due to the small thermal diffusion, it takes a long time to create a polymerization kernel which is initially very curved and takes quite a long time to propagate through the polymeric composite. Although not shown here, the curved polymerization front corresponding to case 3 becomes a nearly planar one upon reaching the top and bottom boundaries. It must be noted that in all the figures illustrating the two-dimensional temperature and monomer concentration profiles at selected times, the horizontal and vertical axes correspond to the x and y axes, respectively.

Fig. 2 illustrates the monomer concentration at the same times as those of Fig. 1 and shows that, even though there are substantial differences initially between cases 1 and 2, i.e., case 1 results in a faster polymerization front than case 2, these two cases exhibit nearly an identical behavior for times greater than about $t = 600$. On the other hand, case 3 results in an initially elongated polymerization front along the y-direction which propagates faster than those of cases

Table 1
Mass/monomer **D** and heat **K** diffusion tensors

Case	D_{11}	K_{11}	D_{22}	K_{22}	D_{12}	K_{12}	D_{21}	K_{21}
1	1	1	1	1	0	0	0	0
2	0.1	1	0.1	1	0	0	0	0
3	1	0.1	1	0.1	0	0	0	0
4	0.1	0.1	0.1	0.1	0	0	0	0
5	1	1	1	0.1	0	0	0	0
6	1	1	0.1	1	0	0	0	0
7	1	1	0.1	0.11	0	0	0	0
8	1	0.1	1	1	0	0	0	0
9	1	0.1	0.1	1	0	0	0	0
10	1	0.1	0.1	0.1	0	0	0	0
11	0.1	1	1	1	0	0	0	0
12	0.1	1	1	0.1	0	0	0	0
13	0.1	1	0.1	0.1	0	0	0	0
14	0.1	0.1	1	1	0	0	0	0
15	0.1	0.1	1	0.1	0	0	0	0
16	0.1	0.1	0.1	1	0	0	0	0
17	1	1	1	1	0.5	0	0.5	0
18	1	1	1	1	0	0.5	0	0.5
19	1	1	1	1	0.5	0.5	0.5	0.5
20	1	1	1	1	0.5	0.5	0	0.5
21	1	1	1	1	0.5	0.5	0	0
22	1	1	1	1	0.5	0.5	0.5	0
23	1	1	1	1	0.5	0	0.5	0.5
24	1	1	1	1	0.5	0	0	0.5
25	1	1	1	1	0.5	0	0	0
26	1	1	1	1	0	0.5	0.5	0.5
27	1	1	1	1	0	0.5	0.5	0
28	1	1	1	1	0	0.5	0	0
29	1	1	1	1	0	0	0.5	0.5
30	1	1	1	1	0	0	0.5	0
31	1	1	1	1	0	0	0	0.5
32	1	1	1	1	0.5	0.1	0.5	0.1
33	1	1	1	1	0.1	0.5	0.1	0.5
34	1	1	1	1	0.1	0.1	0.1	0.1
35	1	1	1	0.1	0.5	0	0.5	0
36	1	0.1	1	1	0.5	0	0.5	0
37	1	1	0.1	1	0	0.5	0	0.5
38	0.1	1	1	1	0	0.5	0	0.5
39	0	1	0	1	0	0	0	0
40	0	0.1	0	0.1	0	0	0	0
41	0	1	0	0.1	0	0	0	0
42	0	0.1	0	1	0	0	0	0
43	0	1	0	1	0	0.1	0	0.1
44	0	1	0	1	0	0.5	0	0.5
45	0	1	0	1	0	0	0	0.5
46	0	1	0	1	0	0.5	0	0

Table 2
Heat of reaction, pre-exponential factor, activation energy and time step

Case	α	β	q	Δt
35	3.52×10^{-2}	40	200	0.01
47	7.04×10^{-2}	40	200	0.01
48	3.52×10^{-2}	30	200	0.01
49	3.52×10^{-2}	40	300	0.01
50	3.52×10^{-2}	40	200	0.005

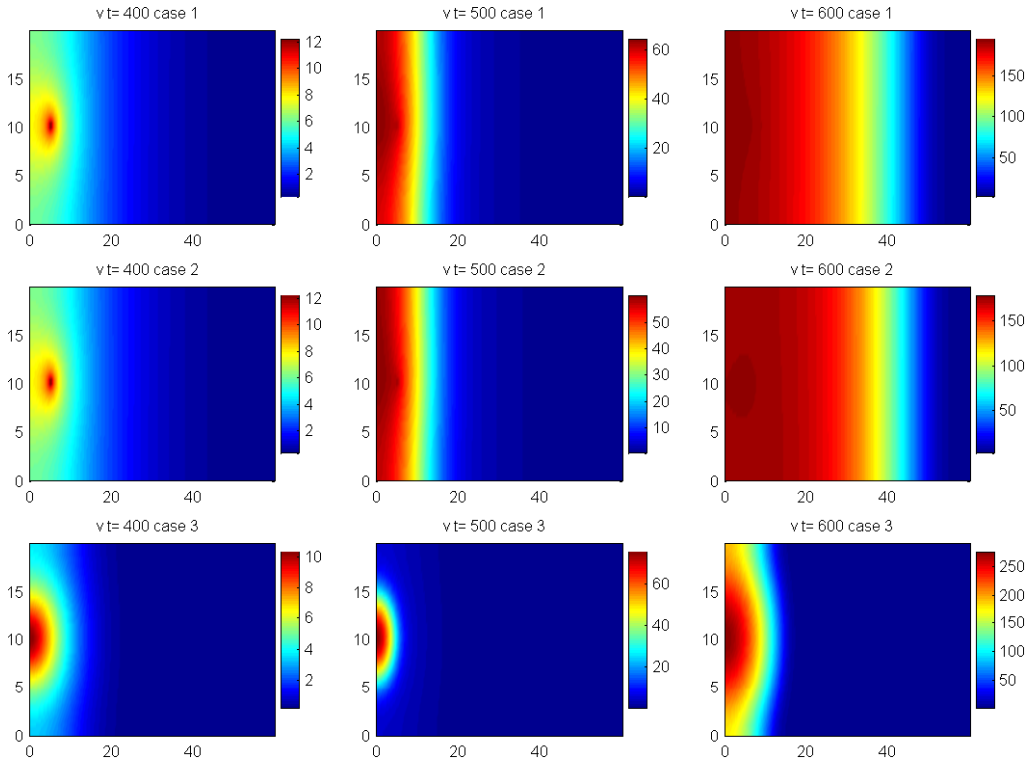

Fig. 1. Temperature profiles at $t = 400$ (left column), 500 (middle column) and 600 (right column) for cases 1 (top row), 2 (middle row) and 3 (bottom row). (The horizontal and vertical axes correspond to the x and y axes, respectively.)

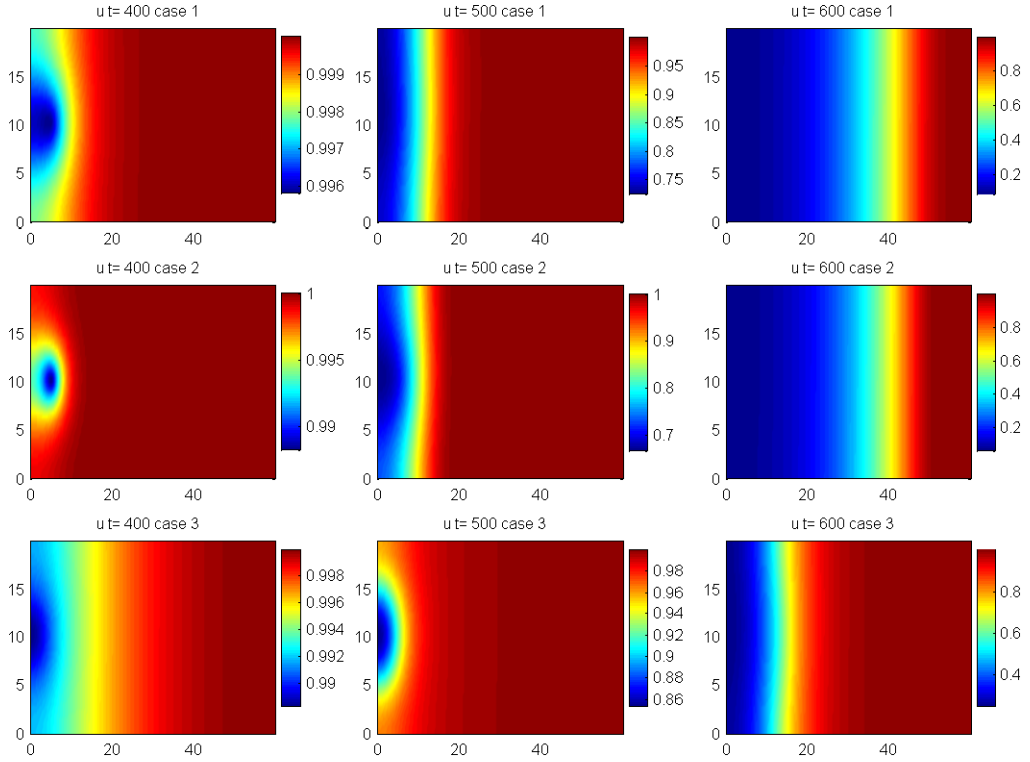

Fig. 2. Monomer mass concentration profiles at $t = 400$ (left column), 500 (middle column) and 600 (right column) for cases 1 (top row), 2 (middle row) and 3 (bottom row). (The horizontal and vertical axes correspond to the x and y axes, respectively.)

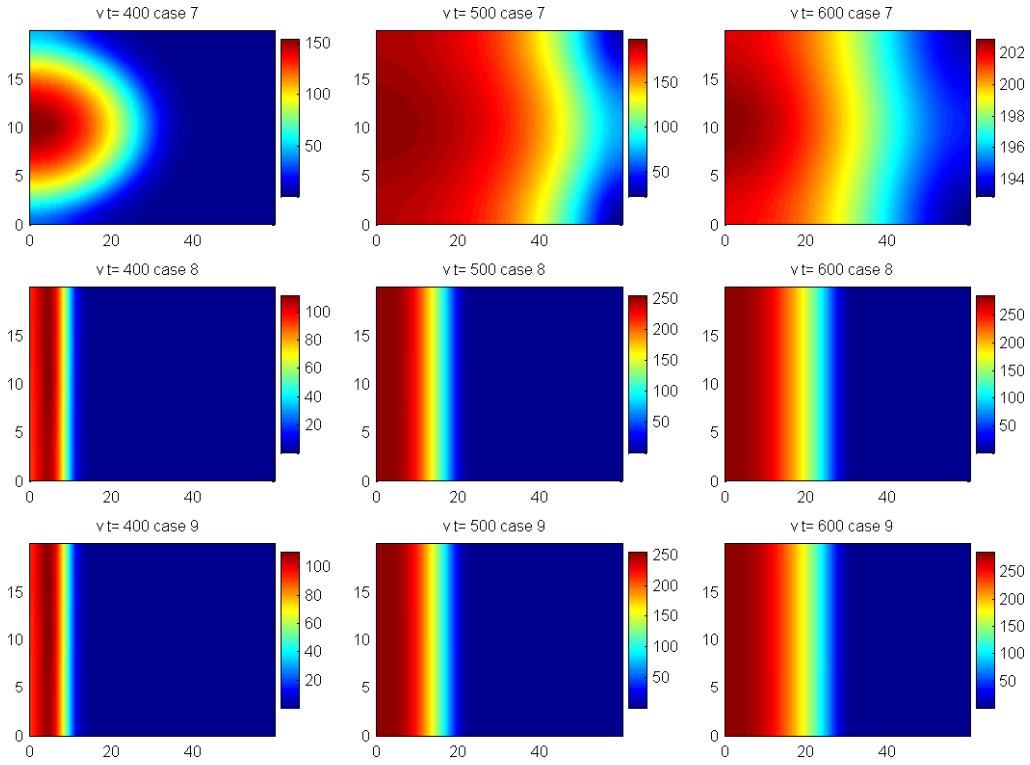

Fig. 3. Temperature profiles at $t = 400$ (left column), 500 (middle column) and 600 (right column) for cases 7 (top row), 8 (middle row) and 9 (bottom row). (The horizontal and vertical axes correspond to the x and y axes, respectively.)

1 and 2, but, later on, the resulting front propagates much slower than in cases 1 and 2 due to a smaller thermal diffusivity.

Figs. 3 and 4 correspond to cases 7, 8 and 9, i.e., orthotropic diffusion tensors. Case 7 is such that the monomer mass and energy diffusion in the x-direction, i.e., D_{11} and K_{11}, is ten times larger than those in the y-direction, i.e., D_{22} and K_{22}, while, in case 8, the thermal diffusion in the y-direction is ten times larger than that in the x-direction. These differences in the components of the diffusion tensors are clearly reflected in Fig. 3 which shows that the temperature profiles for case 7 present a bulge at mid-height, i.e., at $y = 10$, indicating a faster penetration of the polymerization front in the x–direction than in the y one. On the other hand, cases 8 and 9 which have smaller thermal diffusion in the x-direction than in the y one, are elongated along the y axis and advance slowly in the x-direction. Moreover, the results presented in Fig. 3 show again that the magnitude of the monomer mass diffusion is not as important as that of heat since there are very few differences between the results corresponding to cases 8 and 9.

Fig. 4 indicates that, for case 7, the monomer concentration presents an advancing bulge along the middle of the domain, i.e., along $y = 0$, that propagates quite fast along the x-axis and reaches the right boundary of the domain earlier than the polymerization fronts corresponding to cases 8 and 9. In fact, the results presented in Fig. 4 show that almost a complete polymerization has occurred by about $t = 600$ in case 7, whereas, in cases 8 and 9, the polymerization front is roughly located at $x = 30$ at the same time and exhibits a planar shape.

Although not shown here, case 6 results in a faster polymerization front than cases 8 and 9 due to the larger magnitude of K_{11}. In addition, the results presented in Figs. 3 and 4 which correspond to orthotropic diffusion tensors, are in accord with the principal directions of those tensors. It is easily seen that the eigenvalues of an orthotropic tensor coincide with the diagonal components of this tensor, and the principal directions are associated with the x and y axes. By way of contrast, the eigenvalues of an anisotropic tensor depend not only on the diagonal elements but also on the off-diagonal components of this tensor, and the principal directions do not correspond to the coordinate axes as illustrated in Figs. 5 and 6 which correspond to cases 34, 35 and 36.

Fig. 5 indicates that an almost complete polymerization has occurred at $t = 600$ for case 35, but the polymerization front exhibits high curvature even after it reaches the right boundary. The results corresponding to case 35 also indicate that, initially, an almost cylindrical polymerization front propagates from the location where the heat source employed to start the polymerization is placed, but this front does not become a planar one after it reaches the top and bottom boundaries as it occurs in the isotropic cases 1, 2 and 3 discussed above. On the other hand, the results corresponding to case 34 show a slower polymerization front due

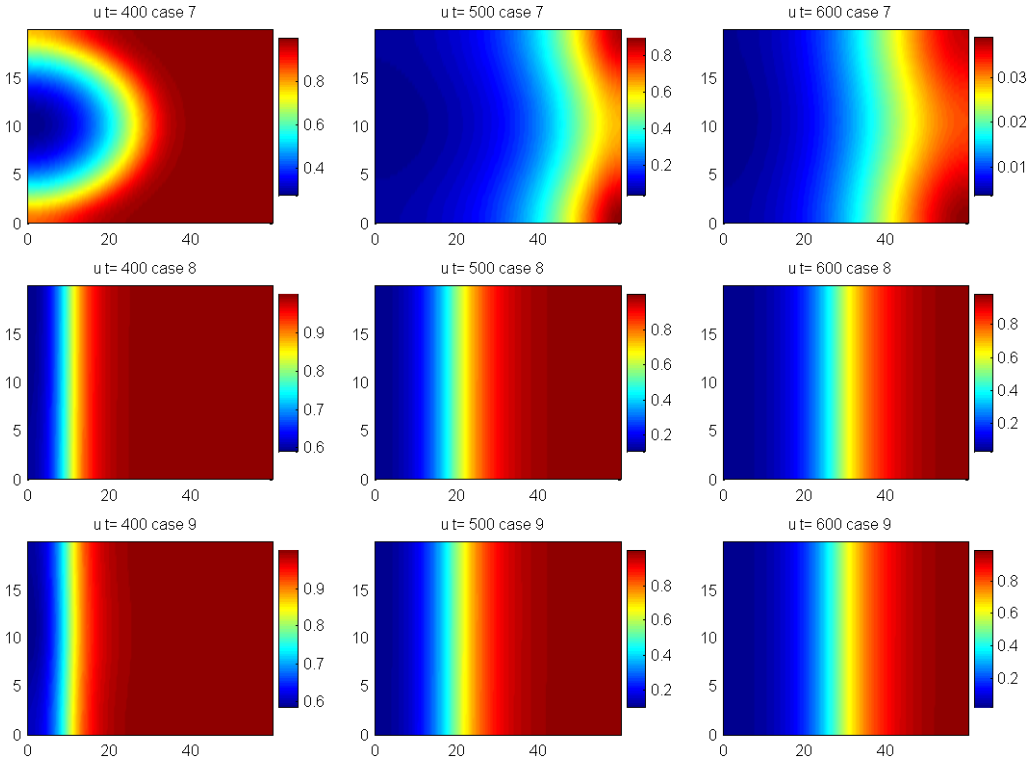

Fig. 4. Monomer mass concentration profiles at $t = 400$ (left column), 500 (middle column) and 600 (right column) for cases 7 (top row), 8 (middle row) and 9 (bottom row). (The horizontal and vertical axes correspond to the x and y axes, respectively.)

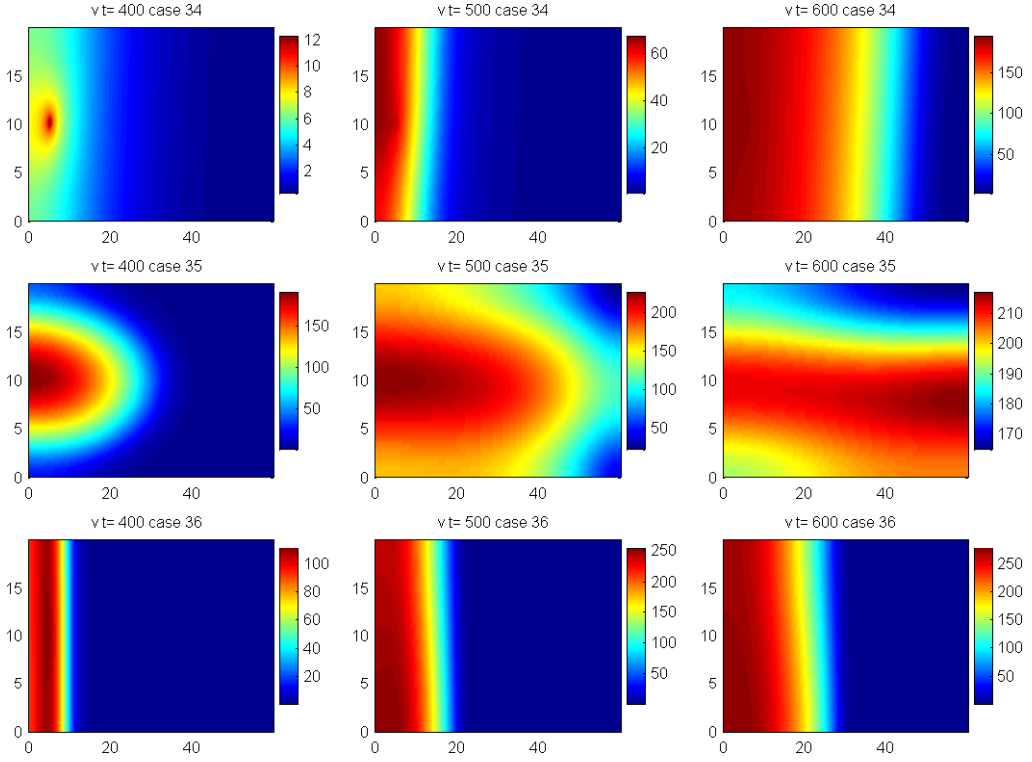

Fig. 5. Temperature profiles at $t = 400$ (left column), 500 (middle column) and 600 (right column) for cases 34 (top row), 35 (middle row) and 36 (bottom row). (The horizontal and vertical axes correspond to the x and y axes, respectively.)

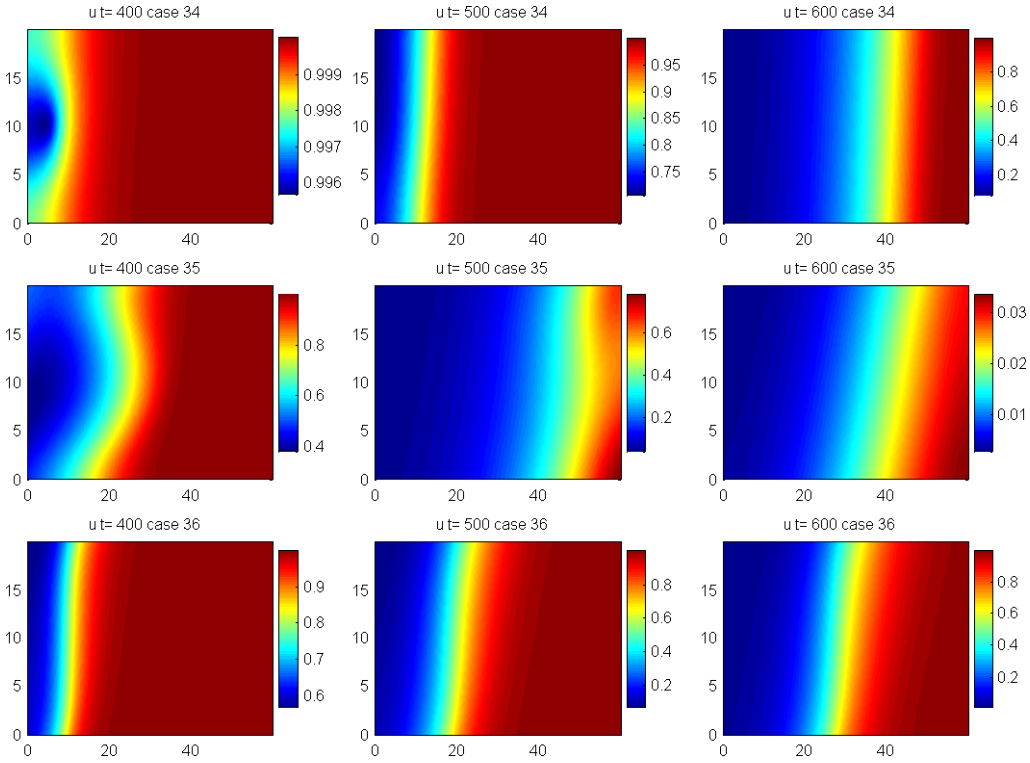

Fig. 6. Monomer mass concentration profiles at $t = 400$ (left column), 500 (middle column) and 600 (right column) for cases 34 (top row), 35 (middle row) and 36 (bottom row). (The horizontal and vertical axes correspond to the x and y axes, respectively.)

to the smaller magnitude of the eigenvalues of the thermal diffusion tensor, and a planar front that forms an angle of less than 90 degrees with the x axis, whereas case 36 results in a slower front than case 34 and this front is inclined more than 90 degrees with respect to the positive x axis. It must be pointed out that the eigenvalues of the thermal diffusion tensors are 1.1 and 0.9 for case 34, and 1 and 0.1 for cases 35 and 36, and, therefore, the principal directions of this tensor form 45 and 135 degrees with the positive x axis for case 34, and 0 and 90 degrees for cases 35 and 36, respectively. On the other hand, the eigenvalues of the monomer mass diffusion tensor are 1.1 and 0.9 for case 34, and 1.5 and 0.5 for cases 35 and 36, respectively, and, therefore, the principal directions of this tensor form 45 and 135 degrees with the positive x axis in case 34, and cases 35 and 36, respectively.

The results presented in Fig. 5 indicate that an almost planar polymerization front propagates along a direction which is inclined less than -45 degrees and more than $+45$ degrees with respect to the x axis in cases 34 and 36, respectively, whereas, in case 35, the front propagates mainly along the x axis but it has a smaller transversal component along the negative y axis. On the other hand, the monomer concentration profiles exhibited in Fig. 6 indicate that the monomer front is inclined at an angle of less than 90 degrees with respect to the positive x axis; this front is almost planar at about $t = 600$ in case 34, exhibits a large curvature in case 35 and shows some curvature in case 36, especially near the top boundary. Fig. 6 also indicates that case 35 results in a faster polymerization front than case 34 which, in turn, exhibits a faster front than case 36.

The results presented in Figs. 1–6 clearly indicate that the monomer mass diffusion tensor does not have a profound effect on the polymerization front of isotropic and orthotropic polymeric composites, but plays a key role in determining the initial polymerization kernel and the initial stages of the propagation of the polymerization front in these materials.

4.2. Thermal degradation without monomer diffusion

In order to further examine the effects of the monomer mass diffusion tensor $\mathbf{D}$ on the polymerization of composites, calculations were also performed with $\mathbf{D} = \mathbf{0}$; these calculations correspond to cases 39–46 of Table 1, and these cases include isotropic, orthotropic and anisotropic thermal diffusion tensors. Note that most of the numerical studies on the curing of polymeric materials performed to-date, e.g., [2], have considered that $\mathbf{D} = \mathbf{0}$, and, therefore, a comparison between results corresponding to $\mathbf{D} = \mathbf{0}$ with those for $\mathbf{D} \neq \mathbf{0}$ allows to determine the effects of the monomer mass diffusion on the thermal degradation of polymeric materials.

The results presented in Fig. 7 indicate that the polymerization time increases as the magnitude of the off-diagonal components of the thermal diffusion tensor is decreased, and the polymerization fronts were found to be almost planar for cases 43, 44 and 45, and formed angles of about 90 and 45

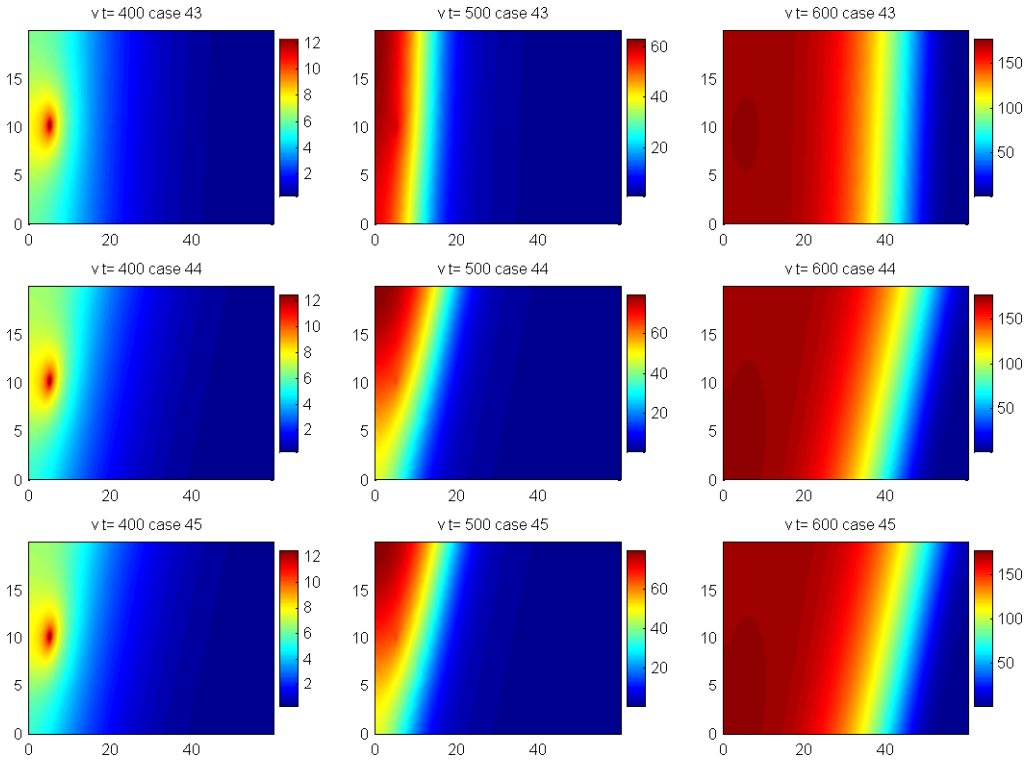

Fig. 7. Temperature profiles at $t = 400$ (left column), 500 (middle column) and 600 (right column) for cases 43 (top row), 44 (middle row) and 45 (bottom row). (The horizontal and vertical axes correspond to the x and y axes, respectively.)

degrees with the positive x axis for case 43 and cases 44 and 45, respectively. On the other hand, case 46 resulted in an almost planar polymerization front. Furthermore, the results presented in Fig. 6 show that very long polymerization times are required when $K_{ii} < 1$.

The results presented in Fig. 8 show the monomer mass concentration at different times as well as the inclination of the polymerization fronts with respect to the x axis. Fig. 8 also indicates that it takes a long time to establish a polymerization kernel, whereas a comparison between the results corresponding to case 39 and case 1 indicates that the monomer mass diffusion tensor plays an important role in determining the initiation of the polymerization reactions, the polymerization kernel and the initial stages of the propagation of the polymerization front, but the final stages of the polymerization are to a large extent independent of the monomer mass diffusion tensor and are mainly controlled by the thermal diffusion tensor.

4.3. Temperature spikes

Figs. 1–8 indicate that the temperature distribution and the monomer concentration are not uniform along the y direction. In addition, it has been found that spiking phenomena may be present in the temperature profiles. These spikes are a consequence of the trapping of the heat generated in the polymerization process, and usually occur in the interior of the domain, although sometimes they also occur very near the boundaries. In order to illustrate the spiking phenomena, we show in Figs. 9 and 10 the profiles of u and v at $y = 10$ as functions of x at three different times. Figs. 9 and 10 correspond to cases 1, 2, 3, 5, 8, 13, 16 and 17 and cases 22, 33, 35, 36, 38, 40, 41, and 42, respectively, and show that the initial temperature profile evolves from the high temperature at the location where the heat source used to start the polymerization is placed, with very little monomer conversion and exhibits spikes at $t = 400$ for cases 1 and 2, whereas no spikes are observed in case 3 at this time. Spikes are not observed for $t \geqslant 500$ in cases 1 and 2 due to the formation of a polymerization front and the no-flux conditions for heat and concentration employed in this paper.

Fig. 9 and other results not presented here indicate that cases 16–18 present spike phenomena at $t = 400$ of about the same magnitude, i.e., $\Delta v \approx 10$, but case 16 shows at higher temperature at $x = 0$ than cases 17 and 18. Although not shown here, spiking phenomena characterized by nearly the same magnitude of the temperature peak and $v(0, 10, t)$ at $t = 400$ as those of Figs. 9 and 10 were also observed in cases 6, 11, 18–34, 37–39 and 43–46 and cases 8, 9, 14, 36, and 42, respectively. Cases 5 and 7 show a temperature spike at an earlier time, and $v(60, 10, t)$ was much smaller than $v(0, 10, t)$ at $t = 600$. The highest value of $v(0, 10, t)$ at $t = 600$ was slightly smaller than 5 for case 10, about 5 for case 15, and about 3 for case 40.

Cases 12, 13, 35 and 41 show a temperature spike at $t < 400$, and $v(60, 10, t)$ was higher than $v(0, 10, t)$ at $t = 600$;

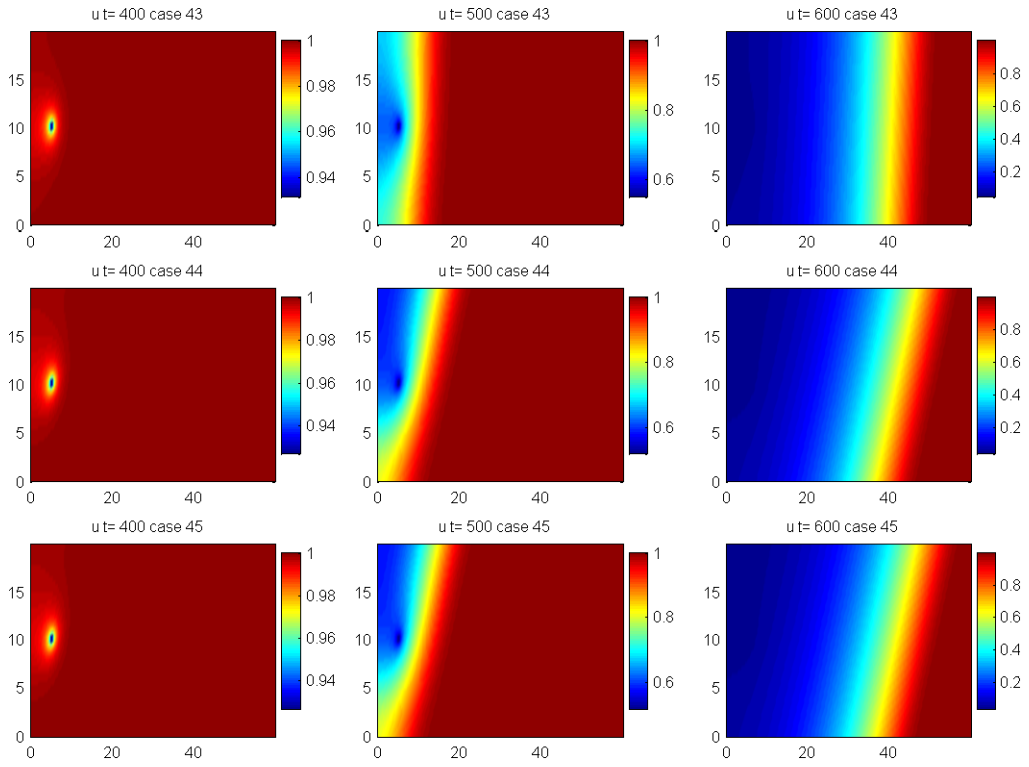

Fig. 8. Monomer mass concentration profiles at $t = 400$ (left column), 500 (middle column) and 600 (right column) for cases 43 (top row), 44 (middle row) and 45 (bottom row). (The horizontal and vertical axes correspond to the x and y axes, respectively.)

in fact, $v(60, 10, t) - v(0, 10, t)$ at $t = 600$ is about 40, 36, 4 and 42 for cases 12, 13, 35 and 41, respectively. As indicated in Table 1, K_{11} is much larger than K_{22} for cases 12 and 13 and, therefore, heat is diffused at a much higher rate in the x direction than in the y direction.

4.4. Temperature and monomer concentration profiles

The nonuniformity of the temperature and monomer concentration profiles are exhibited along the y axis at different times in Figs. 11–14. Fig. 11 correspond to $x = 9.9$ and indicates that very large differences are observed in u and v for cases 1, 2, 3, 5, 8, 13, 16 and 17 at $t \leqslant 500$. In particular, at $t = 400$, the highest peak temperature is associated with case 5 and this is followed by case 13; both cases 5 and 13 exhibit a relative maximum in the temperature profile in the interior of the domain. Cases 8 and 16 result in almost uniform temperature profiles at $t = 400$ and their temperature is higher than that corresponding to cases 1, 3 and 17 at this time. Both the temperature and monomer concentration profiles undergo large changes as a comparison between the results corresponding to $t = 400$ and 500 shows. However, at $t = 600$, the temperature profiles are almost straight lines from $y = 0$ to $y = 20$ characterized by the same temperature at both boundaries for isotropic polymeric materials and a temperature at $y = 30$ lower than that at $y = 0$ for orthotropic and anisotropic ones, except for case 3 that still shows a relative maximum in the temperature profile in the interior of the domain. Similar results to those presented in Fig. 11 have been observed at $x = 20$ as shown in Fig. 12 which illustrates that, at $t = 600$, cases 5 and 13 result in almost complete curing, and cases 1, 2 and 17, case 8 and case 16 have a monomer concentration nearly equal to about 0.32, 0.58 and 0.68, respectively. Fig. 12 also shows that little conversion of monomers has occurred at $t = 600$ for case 3.

Figs. 13 and 14 illustrate the temperature and monomer concentration profiles at $x = 9.9$ and $x = 30$, respectively, along the y axis at different times for cases 22, 33, 35, 36, 38, 40, 41, and 42, show the nonuniformity of the temperature profiles for anisotropic polymeric composites, and indicate that cases 35 and 38 are characterized by a relative maximum in the temperature profile; the peak temperature is larger for case 35 than for case 38, whereas the other cases exhibit more uniform and lower temperature profiles at $t = 400$.

The results at $t = 500$ presented in Fig. 13 are interesting for several reasons. First, case 35 still exhibits a relative maximum in temperature, whereas case 38 now shows a relative minimum. Second, case 40 shows nearly a zero polymerization/curing. Third, cases 22, 35 and 36 are characterized by $v(9.9, 20, 500) < v(9.9, 0, 500)$, whereas the opposite holds for cases 33 and 38. Fourth, the temperatures for most of the cases presented in Fig. 13 are similar at $t = 600$, except for case 36 which has a higher temperature and case 40 which has not started the polymerization at this time. Similar trends to those illustrated in Fig. 13 have

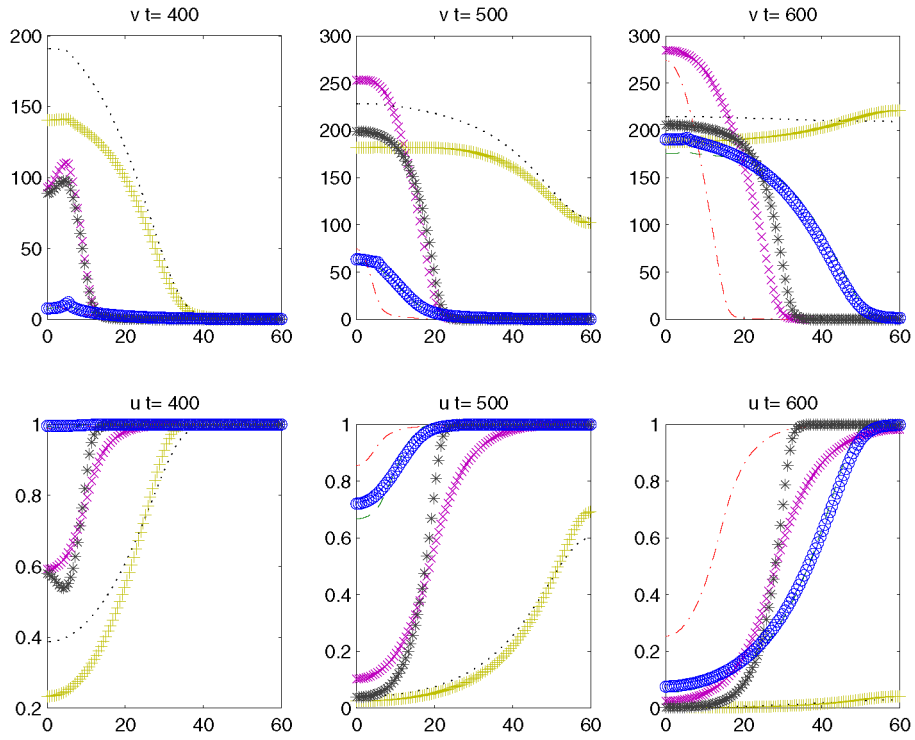

Fig. 9. Nondimensional temperature profiles $v(x, 10, t)$ (top) and monomer concentration $u(x, 10, t)$ (bottom) at $t = 400$ (left column), 500 (middle column) and 600 (right column). Solid line—case 1; dashed line—case 2; dashed–dotted line—case 3; dotted line—case 5; ×—case 8; +—case 13; ∗—case 16; ○—case 17. (The horizontal and vertical axes correspond to the x axis and v or u, respectively.)

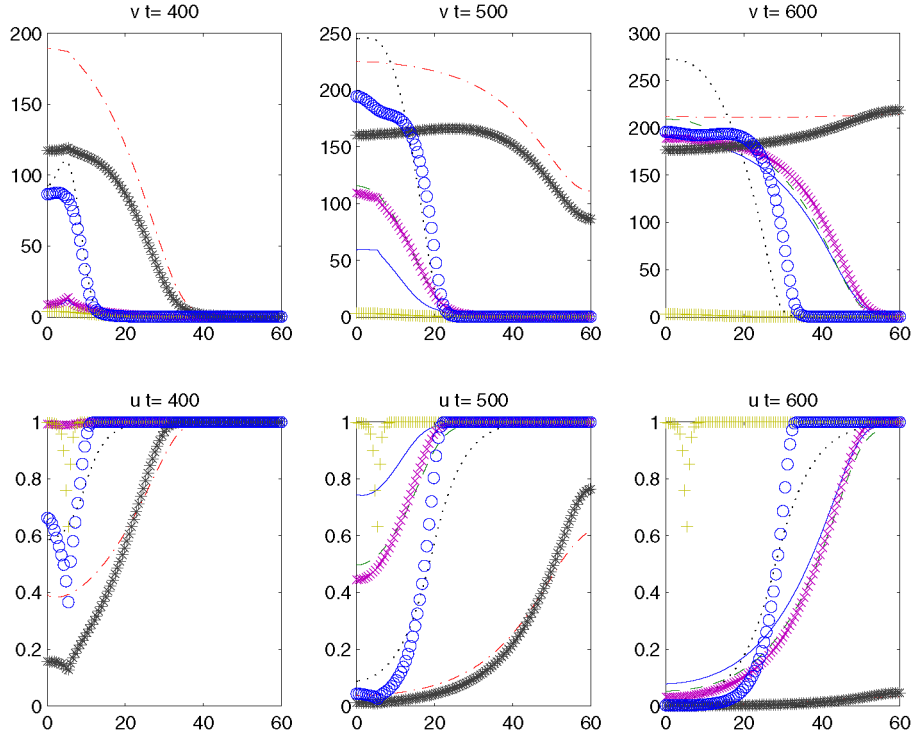

Fig. 10. Nondimensional temperature profiles $v(x, 10, t)$ (top) and monomer concentration $u(x, 10, t)$ (bottom) at $t = 400$ (left column), 500 (middle column) and 600 (right column). Solid line—case 22; dashed line—case 33; dashed–dotted line—case 35; dotted line—case 36; ×—case 38; +—case 40; ∗—case 41; ○—case 42. (The horizontal and vertical axes correspond to the x axis and v or u, respectively.)

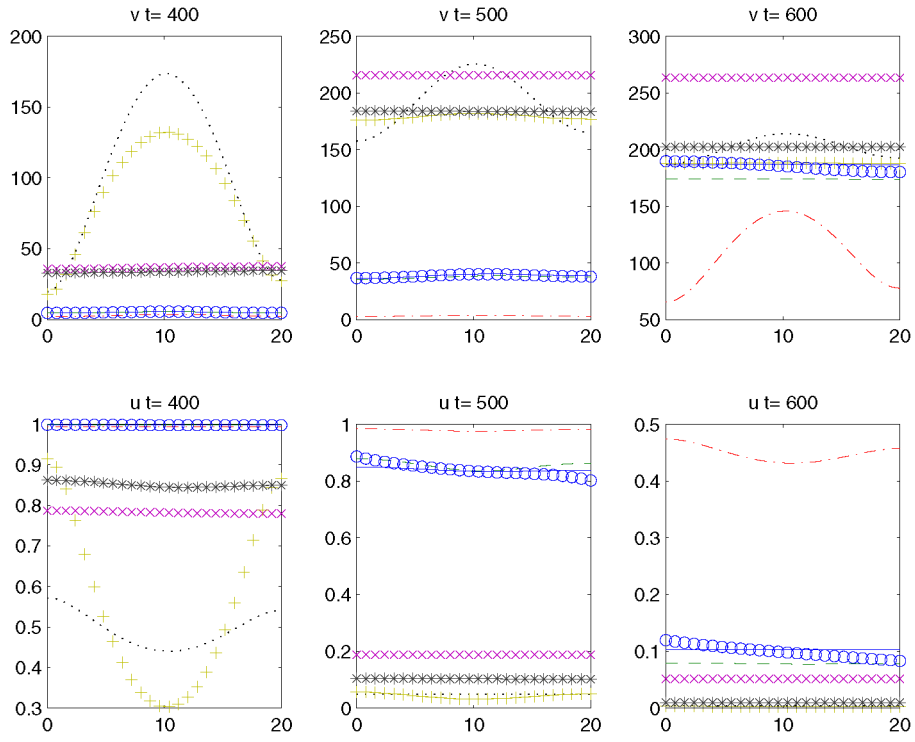

Fig. 11. Nondimensional temperature profiles $v(9.9, y, t)$ (top) and monomer concentration $u(9.9, y, t)$ (bottom) at $t = 400$ (left column), 500 (middle column) and 600 (right column). Solid line—case 1; dashed line—case 2; dashed–dotted line—case 3; dotted line—case 5; ×—case 8; +—case 13; ∗—case 16; ∘—case 17. (The horizontal and vertical axes correspond to the y axis and v or u, respectively.)

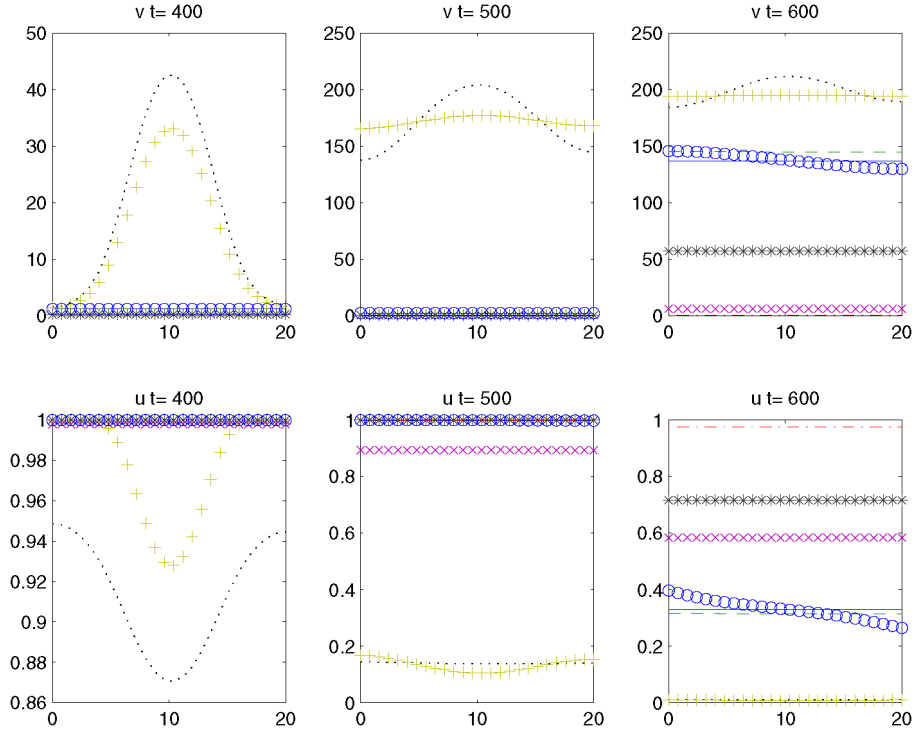

Fig. 12. Nondimensional temperature profiles $v(30, y, t)$ (top) and monomer concentration $u(30, y, t)$ (bottom) at $t = 400$ (left column), 500 (middle column) and 600 (right column). Solid line—case 1; dashed line—case 2; dashed–dotted line—case 3; dotted line—case 5; ×—case 8; +—case 13; ∗—case 16; ∘—case 17. (The horizontal and vertical axes correspond to the y axis and v or u, respectively.)

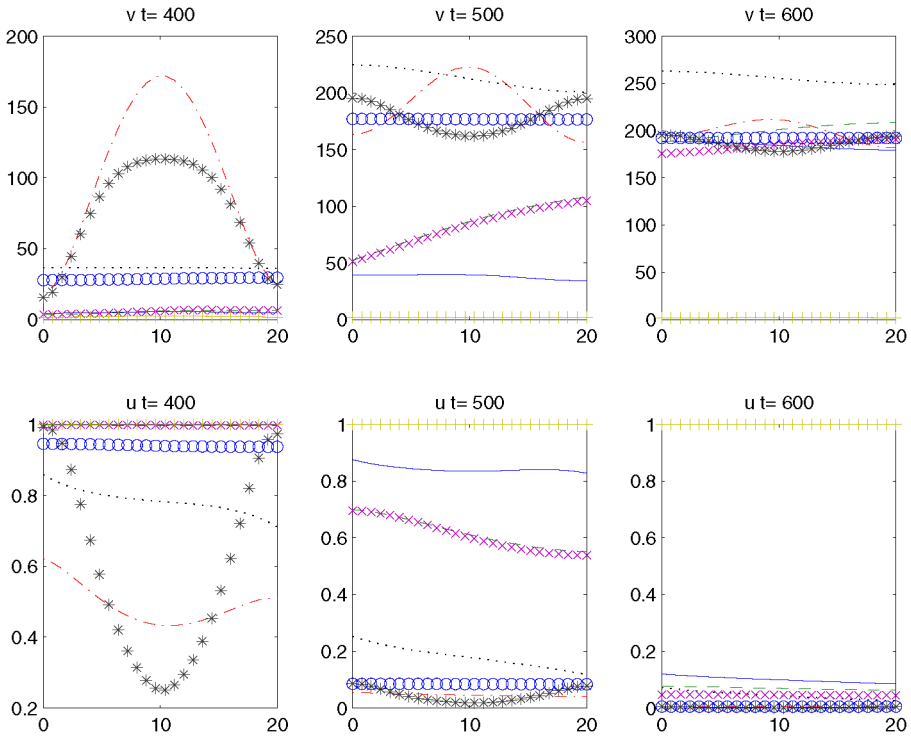

Fig. 13. Nondimensional temperature profiles $v(9.9, y, t)$ (top) and monomer concentration $u(9.9, y, t)$ (bottom) at $t = 400$ (left column), 500 (middle column) and 600 (right column). Solid line—case 22; dashed line—case 33; dashed–dotted line—case 35; dotted line—case 36; ×—case 38; +—case 40; ∗—case 41; ○—case 42. (The horizontal and vertical axes correspond to the y axis and v or u, respectively.)

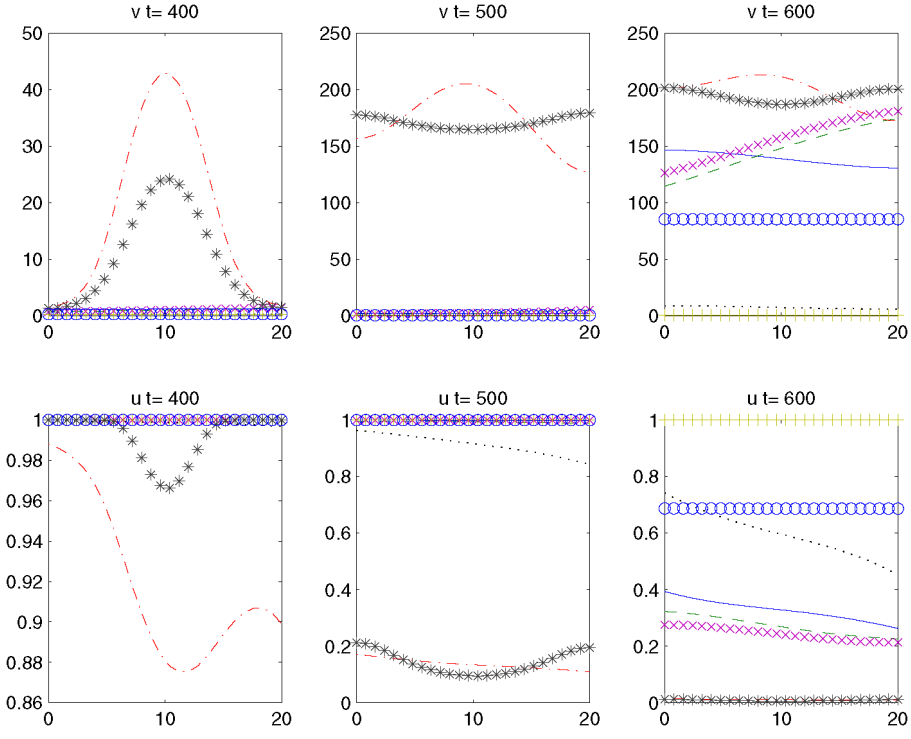

Fig. 14. Nondimensional temperature profiles $v(30, y, t)$ (top) and monomer concentration $u(30, y, t)$ (bottom) at $t = 400$ (left column), 500 (middle column) and 600 (right column). Solid line—case 22; dashed line—case 33; dashed–dotted line—case 35; dotted line—case 36; ×—case 38; +—case 40; ∗—case 41; ○—case 42. (The horizontal and vertical axes correspond to the y axis and v or u, respectively.)

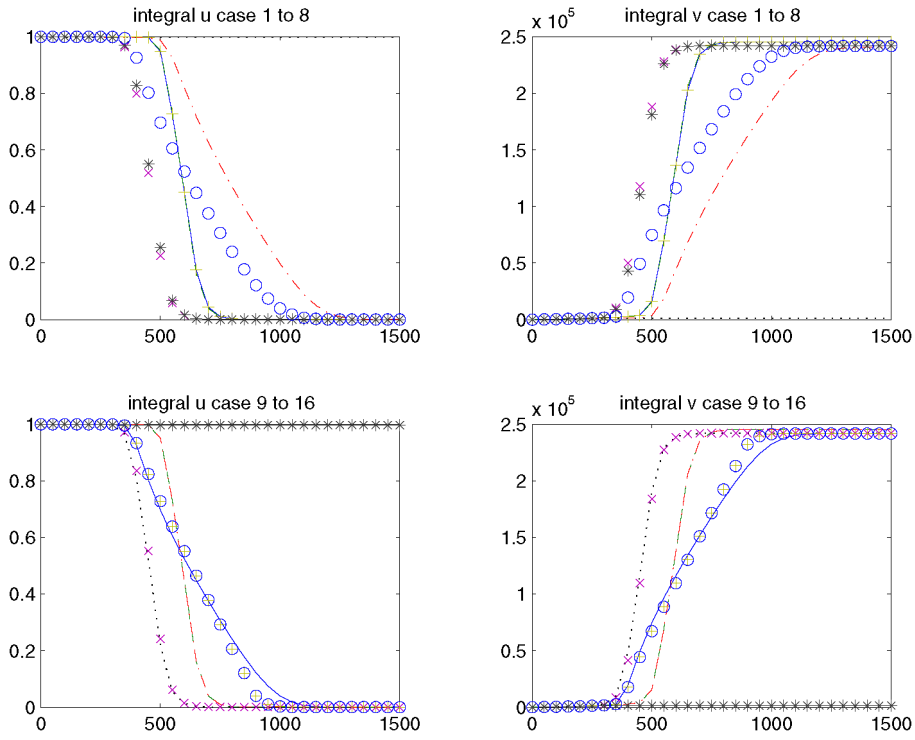

Fig. 15. Monomer conversion rate, CR, and energy, E, as functions of time. (Top: solid line–case 1; dashed line—case 2; dashed–dotted line—case 3; dotted line—case 4; ×—case 5; +—case 6; ∗—case 7; ○—case 8. Bottom: solid line—case 9; dashed line—case 10; dashed–dotted line—case 11; dotted line—case 12; ×—case 13; +—case 14; ∗—case 15; ○—case 16. (The horizontal and vertical axes correspond to t and CR or E, respectively.)

also been observed at $x = 30$ as indicated in Fig. 14. The most noticeable feature of this figure is the relative minimum and the relative maximum exhibited by the monomer concentration profile at $t = 400$ for case 35, as well the effects of the anisotropy of the heat and monomer diffusion tensors on the temperature profiles and, especially, on the difference $v(30, 30, t) - v(30, 0, t)$.

As stated before, the physics of the polymerization processes is governed by heat and kinetics phenomena, and there are two competing requirements in this nonlinear coupling, i.e., maximizing the degree of curing and minimizing the temperature spikes. As shown in Figs. 1–10, the dynamics of the temperature spikes are intimately related to the conversion rate of the monomers, and one could try to control the thermal spikes by exposing the polymeric composite to additional heat sources such as, for example, laser irradiation [17]. In fact, stereolithography is based on curing polymers by exposing small zones to laser irradiation.

4.5. Monomer conversion rates and polymerization times

The integrals of both the monomer concentration (normalized with respect to its initial value) and the temperature with respect to space, i.e.,

$$CR(t) = \int_0^{L_x}\int_0^{L_y} u(x, y, t)\,\mathrm{d}x\,\mathrm{d}y \Big/ \int_0^{L_x}\int_0^{L_y} u(x, y, 0)\,\mathrm{d}x\,\mathrm{d}y \qquad (8)$$

$$E(t) = \int_0^{L_x}\int_0^{L_y} v(x, y, t)\,\mathrm{d}x\,\mathrm{d}y \qquad (9)$$

are exhibited in Figs. 15–17. Fig. 15 shows that the polymerization is nearly identical for cases 1 and 2 and for cases 3 and 4; the latter show a less steep (temporal) gradient than the former on account of the smaller component of the thermal diffusion tensor in the x direction for cases 3 and 4. The polymerization curves are nearly identical for cases 5 and 6, cases 7 and 10, and cases 8 and 9. Cases 5 and 6 exhibit smaller polymerization times than cases 7–10; cases 7 and 10 have conversion rates which are nearly parallel to those of cases 5 and 6; cases 5, 6, 7 and 10 have a steeper conversion rate and shorter polymerization times than cases 8 and 9.

Cases 12 and 13 are characterized by smaller polymerization times than case 11 which, in turn, requires smaller polymerization times than cases 14 and 16. The conversion rate for case 11 is nearly parallel to that of cases 12 and 13, and these three cases have steeper conversion rates than cases 14 and 16. For the initiation model of the polymerization employed in this paper, it has been found that case 15 does not result in any polymerization; this result is not surprising in view of the fact that the components of the thermal diffusion tensor of this case are small and the component of the monomer mass diffusion tensor in the x direction is smaller than that in the y direction.

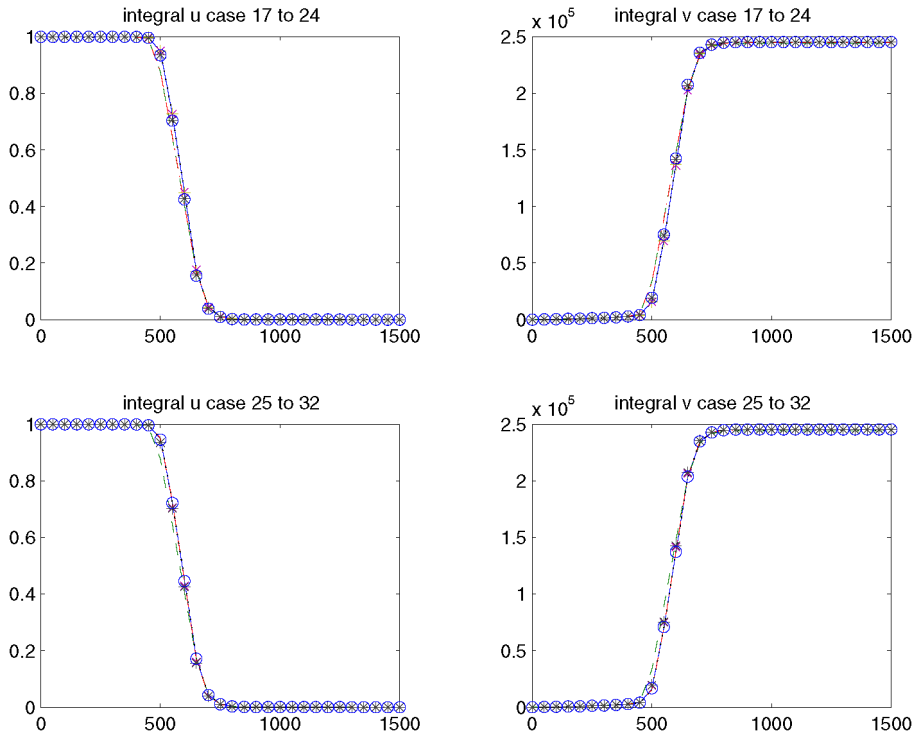

Fig. 16. Monomer conversion rate, CR, and energy, E, as functions of time. (Top: solid line—case 17; dashed line—case 18; dashed–dotted line—case 19; dotted line—case 20; ×—case 21; +—case 22; ∗—case 23; ○—case 24. Bottom: solid line—case 25; dashed line—case 26; dashed–dotted line—case 27; dotted line—case 28; ×—case 29; +—case 30; ∗—case 31; ○—case 32. (The horizontal and vertical axes correspond to t and CR or E, respectively.)

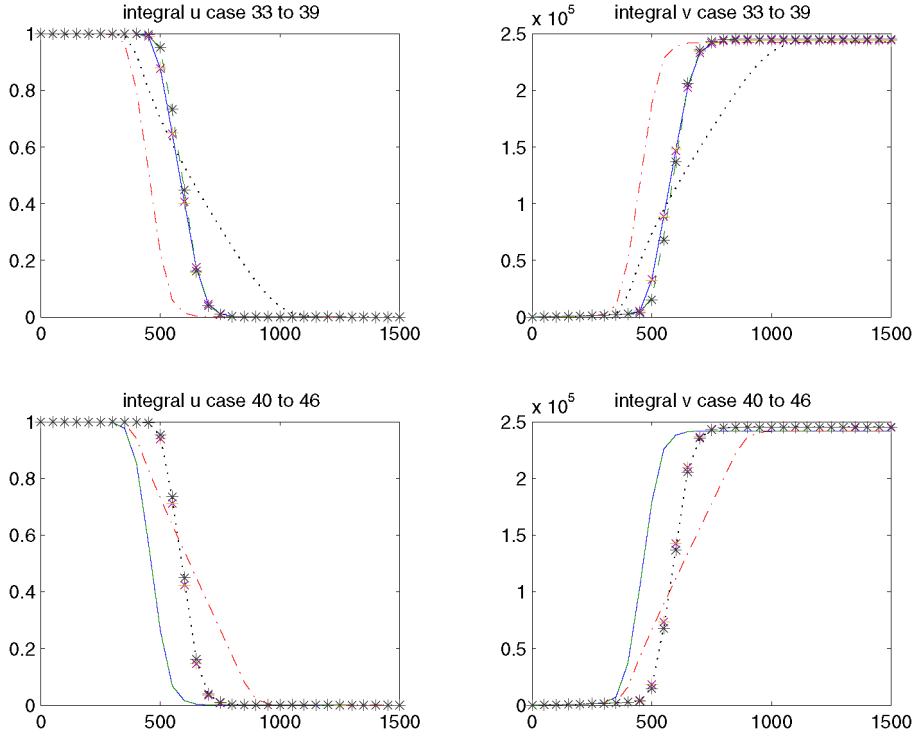

Fig. 17. Monomer conversion rate, CR, and energy, E, as functions of time. (Top: solid line—case 33; dashed line—case 34; dashed–dotted line—case 35; dotted line—case 36; ×—case 37; +—case 38; ∗—case 39. Bottom: solid line—case 40; dashed line—case 41; dashed–dotted line—case 42; dotted line—case 43; ×—case 44; +—case 45; ∗—case 46. (The horizontal and vertical axes correspond to t and CR or E, respectively.)

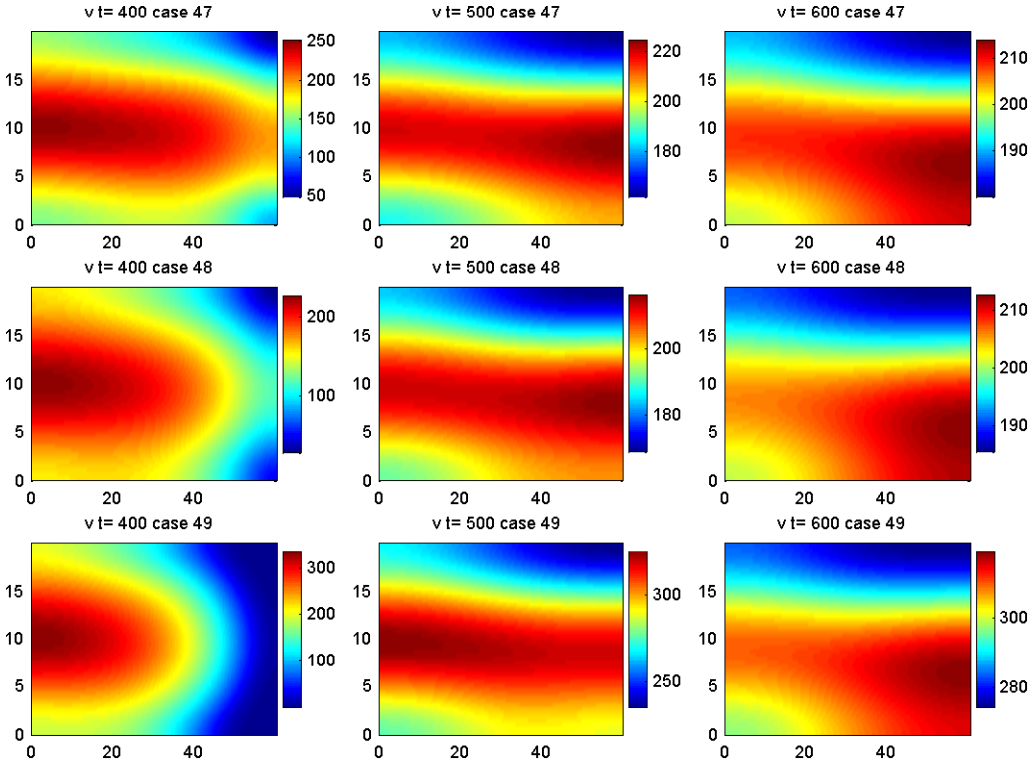

Fig. 18. Temperature profiles at $t = 400$ (left column), 500 (middle column) and 600 (right column) for cases 47 (top row), 48 (middle row) and 49 (bottom row). (The horizontal and vertical axes correspond to the x and y axes, respectively.)

The differences in conversion rates for cases 17–22 are small, except at the beginning of the polymerization process and during the formation of the polymerization kernel. Once a polymerization front has been formed, the differences between the results corresponding to cases 17–22 are small, despite the differences in the off-diagonal components of the heat and monomer mass diffusion tensors in these cases. Therefore, taking into consideration the time evolution of the monomer concentration and temperature, it may be concluded that the conversion rate is nearly independent of the off-diagonal components of the heat and monomer mass diffusion tensors if the diagonal components of these tensors are equal to unity. A similar comment applies to the conversion rates for cases 23–28 and cases 29–34.

Case 35 shows a smaller polymerization time than cases 37 and 38 which, in turn, exhibit a faster polymerization than case 36. The conversion rate for cases 37 and 38 is nearly parallel to that of case 35 and the conversion rates of these three cases are steeper than that for case 36. This can again be justified by the smaller component of the thermal diffusion tensor in the x direction for case 36 than for cases 35, 37 and 38.

Cases 40 and 41 yield almost the same monomer conversion rates and polymerization times. A similar comment applies to cases 39, 43 and 46 which show longer polymerization times than and almost parallel conversion rates to those of cases 40 and 41. Case 39, in turn, results in a shorter polymerization time and a steeper conversion rate than case 42.

4.6. Effects of the heat of reaction, pre-exponential factor and activation energy

In the results presented in previous paragraphs, $q = 200$, $\alpha = 3.52 \times 10^{-2}$, $\beta = 40$, i.e., the heat of reaction, the pre-exponential factor and the activation energy of the chemical reaction were assumed to be identical for all the cases considered. In this subsection, we study the effects of q, α, β and Δt for the same heat and monomer mass diffusion tensors as case 35 of Table 1, by varying one parameter at a time as indicated in Table 2, and some sample results are presented in Figs. 18 and 19.

Fig. 18 shows that case 47 results in a faster polymerization than cases 48 and 49 as indicated in the temperature profiles at $t = 400$; the latter, in turn, result in a faster front than case 35, cf. Fig. 5. Therefore, the results presented in Figs. 5 and 18 indicate that, for the heat and monomer mass diffusion tensors of case 35, the pre-exponential factor has a larger effect on the polymerization front location than the activation energy and the heat of reaction at $t = 400$; however, case 49 results in higher temperatures than cases 47, 48 and 35 at $t = 400$. Figs. 5 and 18 also indicate that the temperature profiles at $t = 600$ exhibit the same trends for cases 35 and 47–49, but case 49 results in the highest temperature.

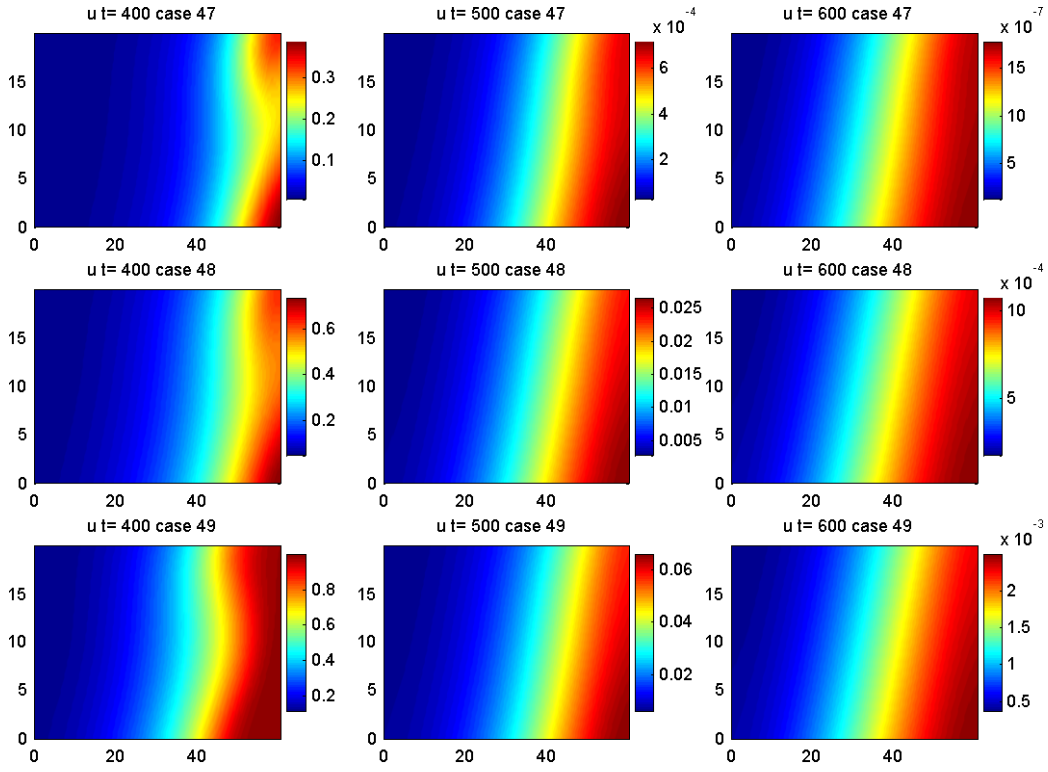

Fig. 19. Monomer mass concentration profiles at $t = 400$ (left column), 500 (middle column) and 600 (right column) for cases 47 (top row), 48 (middle row) and 49 (bottom row). (The horizontal and vertical axes correspond to the x and y axes, respectively.)

The results presented in Fig. 5 for case 35 and Fig. 18 are in accord with the physics of a one-step chemical reaction such as the one employed in this paper, for an increase in either the pre-exponential factor or the heat of reaction and a decrease in the activation energy are expected to result in faster polymerization fronts. The results shown in these figures indicate that α and β play a more important role in determining the polymerization time than q, whereas an increase in q results in larger temperatures than a similar increase in α or a similar decrease in β.

The effects of α, β and q on the monomer concentration profiles at selected times are exhibited in Fig. 6 for case 35 and Fig. 19. These figures indicate that cases 47–49 result in faster polymerization fronts than case 35; cases 47–49 also result in smaller monomer concentration at $t = 600$ than case 35.

In order to emphasize the effects of α, β, q and Δt on the thermal degradation of polymeric materials, we show in Figs. 20 and 21 the temperature (top) and monomer concentration (bottom) at selected times along $y = 10$ and $x = 9.9$, respectively. These figures also illustrate the effects of the anisotropy of the heat and monomer mass diffusion tensors as functions of the aforementioned parameters.

Fig. 20 shows that, for the cases considered in Table 2, the results corresponding to $\Delta t = 0.005$ are indistinguishable from those corresponding to $\Delta t = 0.01$, case 49 results in less uniform temperature profiles than cases 47 and 48 at $t = 400$, cases 47–49 require less time to achieve almost uniform temperature profiles than case 35 as indicated at $t = 400$ and 500, the temperature profiles are almost uniform at $t = 600$, case 49 results in higher temperature at $t = 600$ than cases 35, 47 and 48, an almost complete polymerization can be observed at $t = 600$ for case 47, case 35 has not reached complete polymerization at $t = 600$, and the largest nonuniformities in the monomer concentration can be observed in cases 35, 48 and 47. Fig. 20 also illustrates that the temperature and monomer concentration profiles at $t = 400$, 500 and 600 along x for $y = 10$ are monotonic functions of x and exhibit relative extrema at $x = 0$ and $x = L_x$. By way of contrast, the temperature profiles along y for $x = 9.9$ shown in Fig. 21 are not monotonic functions of y and exhibit a relative maximum which is also a supremum at about $y = 10$. Moreover, the temperature profiles shown in Fig. 21 are not symmetric with respect to $y = 10$ and exhibit relative minima at $y = 0$ and $y = L_y$. The temperature at $y = 0$ increases as time increases and is larger than that at $y = L_y$ at $t = 600$ for cases 35 and 47–49.

The asymmetry in the temperature profiles shown in Fig. 21 can also be observed in the monomer concentration profiles exhibited in the same figure which shows that, for cases 47–50, the monomer concentration along the y axis for $x = 9.9$ exhibits relative extrema at $y = 0$ and $y = L_y$ but decreases in a monotonic fashion with y at $t = 400$, 500 and 600. This monotonic behavior can also be observed for case 35 at $t = 500$ and 600, whereas cases 35 and 50 result in monomer concentration profiles characterized by relative

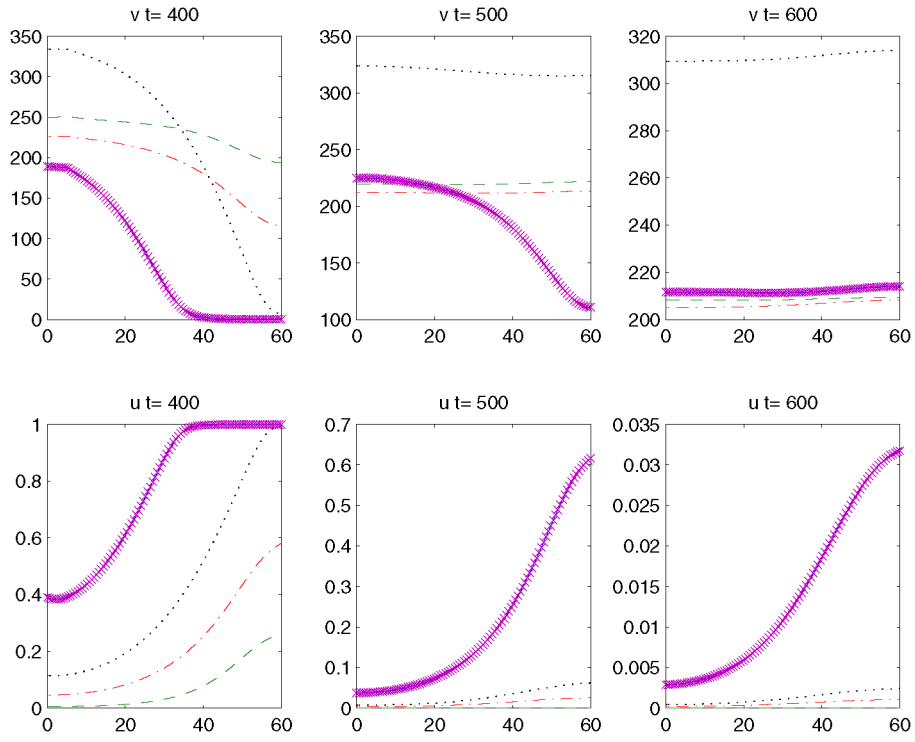

Fig. 20. Nondimensional temperature profiles $v(x, 10, t)$ (top) and monomer concentration $u(x, 10, t)$ (bottom) at $t = 400$ (left column), 500 (middle column) and 600 (right column). Solid line—case 35; dashed line—case 47; dashed–dotted line—case 48; dotted line = case 49; ×—case 50. (The horizontal and vertical axes correspond to the x axis and v or u, respectively.)

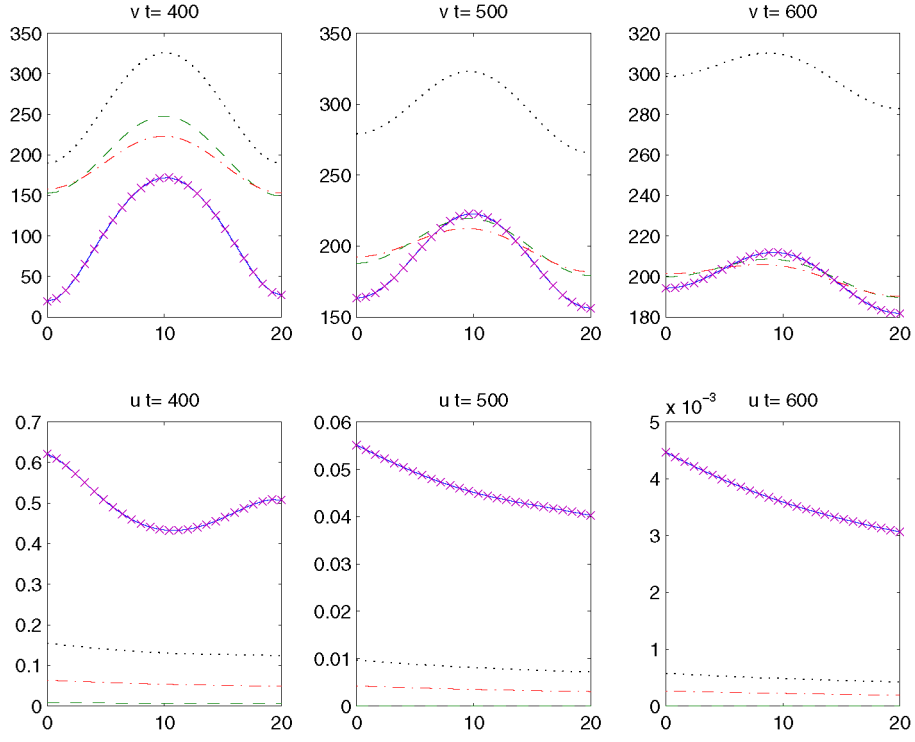

Fig. 21. Nondimensional temperature profiles $v(9.9, y, t)$ (top) and monomer concentration $u(9.9, y, t)$ (bottom) at $t = 400$ (left column), 500 (middle column) and 600 (right column). Solid line—case 35; dashed line—case 47; dashed–dotted line—case 48; dotted line—case 49; ×—case 50. (The horizontal and vertical axes correspond to the y axis and v or u respectively, respectively.)

maxima at $y = 0$ and $y = L_y$ and a relative minimum at about $y = 10$ at $t = 400$.

The results presented in this paper and, especially, those illustrated in Figs. 18–21 clearly show that an accurate prediction of the thermal degradation of polymeric materials requires an accurate knowledge of the pre-exponential factor, activation energy and heat of reaction in order to determine accurately the polymerization times and the temperature distribution and avoid high temperature gradients that may result in cured composites with large nonuniformities or residual stresses. The results presented here also indicate that the anisotropy of the heat and monomer mass diffusion tensors plays a paramount role in determining the initial polymerization kernel, the polymerization front propagation, and the temperature distribution. Since the dynamics of the temperature spikes are intimately related to the conversion rate of the monomers which, in turn, is affected by the polymerization reactions and the anisotropy of the heat and monomer mass diffusion tensors, one could try to control the thermal spikes by exposing the polymeric composite to additional heat sources such as, for example, laser irradiation [17].

5. Conclusions

A second-order accurate, linearly-implicit, time-linearized finite difference method has been developed to study the thermal degradation/curing of polymeric composites in two-dimensions as a function of the monomer/mass and heat diffusion tensors for the case of a simple first-order polymerization kinetics and an Arrhenius law that does not exhibit the cold-boundary difficulty for the initial conditions employed in this study.

It has been found that the monomer mass diffusion tensor does not play an important role in determining the final stages of the polymerization and the curing time for both isotropic and orthotropic polymeric materials, although it affects strongly the initiation of the polymerization kinetics, the formation of the polymerization kernel and the initial stages of the propagation of the polymerization front. However, the anisotropy of the mass/monomer diffusion tensor plays a paramount role in determining the shape, direction and velocity of the polymerization front if the thermal diffusion tensor is also anisotropic. In this case, it has been found that, depending on the magnitude of the off-diagonal components of these tensors, the polymerization front may exhibit either a high curvature even after it has reached the top and bottom boundaries or a planar shape which is inclined with respect to the x direction. The curvature and inclination of this front as well as the polymerization time are found to be very sensitive to the magnitude of the components of the monomer mass and heat diffusion tensors. Although, in some cases, it was possible to draw an almost direct correspondence between the principal directions of the thermal diffusion tensor and the orientation and propagation of the polymerization front, it was found to be nearly impossible to draw a similar correspondence when both the monomer mass and heat diffusion tensors are strongly anisotropic and their components are of the same magnitude.

Acknowledgements

This research was partially financed by Project BFM2001-1902 from the Ministerio de Ciencia y Tecnología of Spain and fondos FEDER. A shorter version of this paper was presented at CHT-04: International Symposium on Advances in Computational Heat Transfer, held on board of MS Midnatsol on the coast of Norway on 19–24 April 2004. The authors kindly appreciate the recommendation of Professor Graham de Vahl Davis of the University of New South Wales, Australia, organizer of the symposium, to submit this paper to this journal. They are also grateful to the referees, whose comments have resulted in an improvement of the presentation.

References

[1] J.S. Tokarski, A.J. Hopfinger, J.D. Hobbs, D.M. Ford, J.-L.M. Faulon, Molecular modelling of polymers, Comput. Theor. Polymer Sci. 7 (1997) 199–214.
[2] R.V.N. Melnik, Computationally efficient algorithms for modelling thermal degradation and spiking phenomena in polymeric materials, Comput. Chem. Engrg. 27 (2003) 1473–1484.
[3] S.P. Kinsey, A. Haji-Sheikh, D.Y.S. Lou, A thermal model for cure of thermoset composites, J. Mater. Process. Technol. 63 (1997) 442–449.
[4] R.H. Halvorson, R.L. Erickson, C.L. Davidson, Energy dependent polymerization of resin-based composites, Dental Mater. 18 (2002) 463–469.
[5] A. Maffezzoli, R. Terzi, Effect of irradiation intensity on the isothermal photopolymerization kinetics of acrylic resins for stereolithography, Thermochimica Acta 321 (1998) 111–121.
[6] A. Nzihou, P. Sharock, A. Ricard, Reaction kinetics and heat transfer studies in thermoset resins, Chem. Engrg. J. 72 (1999) 53–61.
[7] W. Köhler, S. Wiegand, Thermal Nonequilibrium Phenomena in Fluid Mixtures, Springer, New York, 2002.
[8] J.I. Ramos. Implicit factorization techniques for two-dimensional, anisotropic, reactive–diffusive media with cross-diffusion effects, Internat. J. Comput. Engrg. Sci. (2003), in press.
[9] J.I. Ramos, Reactive–diffusive phenomena in two-dimensional, anisotropic media, Internat. J. Numer. Methods Heat Fluid Flow 13 (2003) 997–1030.
[10] S.K. Kim, D.-H. Kim, I.M. Daniel, Optimal control of accelerator concentration for resin transfer molding process, Internat. J. Heat Mass Transfer 46 (2003) 3747–3754.
[11] A. Abbassi, M.R. Shahnazari, Numerical modeling of mold filling and curing in non-isothermal RTM process, Appl. Therm. Engrg. 24 (2004) 2453–2465.
[12] F.A. Williams, Combustion Theory, second ed., Benjamin/Cummings Publishing Company, Menlo Park, CA, 1985.
[13] Ya.B. Zeldovich, G.I. Barenblatt, V.B. Librovich, G.M. Makhviladze, The Mathematical Theory of Combustion and Explosions, Consultants Bureau, A Division of Plenum Publishing Company, New York, 1985.
[14] A.G. Merzhanov, Combustion and explosion processes in physical chemistry and technology of inorganic materials, Russian Chem. Rev. 72 (2003) 289–310.

[15] A.A. Borisov, L. De Luca, A. Merzhanov, Self-Propagating High-Temperature Synthesis of Materials, Taylor & Francis, New York, 2002.
[16] D.S. Huh, M.S. Kim, S.J. Choe, Free radical polymerization of diacrylate by thermal front, Bull. Korean Chem. Soc. 22 (2001) 769–771.
[17] W. Hong, Y.T. Lee, H. Gong, Thermal analysis of layer formation in a stepless rapid prototyping process, Appl. Therm. Engrg. 24 (2004) 255–268.
[18] V.M. Ilyashenko, J.A. Pojman, Single-head spin modes in frontal polymerization, Chaos 8 (1998) 285–289.
[19] E.F. Costa, P.L.C. Lage, E.C. Biscaia, On the numerical solution and optimization of styrene polymerization in tubular reactors, Comput. Chem. Engrg. 27 (2003) 1591–1604.
[20] M.F. Perry, V.A. Volpert, Linear stability analysis of two monomer systems of frontal polymerization, Chem. Engrg. Sci. 59 (2004) 3451–3460.
[21] L.R. Ritter, W.E. Olmstead, V.A. Volpert, Initiation of free-radical polymerization waves, SIAM J. Appl. Math. 63 (2003) 1831–1848.
[22] H.W. So, A. Taube, Modelling and experimental investigation of microwave heating of adhesively bonded polypropylene joint, Internat. J. Adhesion & Adhesives 24 (2004) 307–312.
[23] V. Kosar, Z. Gomzi, In-depth analysis of the mathematical model of polyester thermosets curing, European Polymer J. 40 (2004) 2793–2802.
[24] T.-L. Li, Simulation of the postexposure bake process of chemically amplified resists by reaction–diffusion equations, J. Comput. Phys. 173 (2001) 348–363.
[25] R. Barrett, M. Berry, T.F. Chan, J. Demmel, J. Donato, J. Dongarra, V. Eijkhout, R. Pozo, C. Romine, H. Van de Vorst, Templates for the Solution of Linear Systems: Building Blocks for Iterative Methods, SIAM, Philadelphia, PA, 1994.
[26] J.I. Ramos, Linearization methods for reaction–diffusion equations: 1-D problems, Appl. Math. Comput. 88 (1997) 199–224.
[27] J.I. Ramos, Linearization methods for reaction–diffusion equations: multidimensional problems, Appl. Math. Comput. 88 (1997) 225–254.
[28] J.I. Ramos, Linearized factorization techniques for multidimensional reaction–diffusion equations, Appl. Math. Comput. 100 (1999) 201–222.